Isogeometric locking-free plate element: a simple first order shear deformation theory for functionally graded plates

Shuohui Yin[a], Jack S. Hale[b], Tiantang Yu[a,*], Tinh Quoc Bui[c,*], Stéphane P.A. Bordas[b,d]

[a] *Department of Engineering Mechanics, Hohai University, Nanjing 210098, P.R. China.*

[b] *Faculté des Sciences, de la Technologie et de la Communication, University of Luxembourg, 6, rue Richard Coudenhove-Kalergi, L-1359, Luxembourg.*

[c] *Department of Mechanical and Environmental Informatics, Graduate School of Information Science and Engineering, Tokyo Institute of Technology, 2-12-1-W8-22, Ookayama, Meguro-ku, Tokyo 152-8552, Japan.*

[d] *Cardiff School of Engineering, Cardiff University, The Queen's Building, The Parade, Cardiff, Wales, CF24 3AA, UK.*

Abstract

An effective, simple, and locking-free plate formulation is proposed to analyze the static bending, buckling, and free vibration of homogeneous and functionally graded plates. The simple first-order shear deformation theory (S-FSDT), which was recently presented in *Composite Structures (2013; 101:332-340)*, is naturally free from shear-locking and captures the physics of the shear-deformation effect present in the original FSDT, whilst also being less computationally expensive due to having fewer unknowns. The S-FSDT requires C^1-continuity that is simple to satisfy with the inherent high-order continuity of the non-uniform rational B-spline (NURBS) basis functions, which we use in the framework of isogeometric analysis (IGA). Numerical examples are solved and the results are compared with reference solutions to confirm the accuracy of the proposed method. Furthermore, the effects of boundary conditions, gradient index, and geometric shape on the mechanical response of functionally graded plates are investigated.

Keywords: *Functionally graded materials; First-order shear deformation theory; Isogeometric analysis; NURBS; Plates*

[*]Corresponding authors. Tel.: +86 2583787901 (T.T. Yu); +81 357343587 (T.Q. Bui).

E-mail addresses: tiantangyu@hhu.edu.cn (T.T. Yu), tinh.buiquoc@gmail.com (T.Q. Bui).

1. Introduction

Functionally graded plates (FG plates) are a special type of composite structures with continuous variation of material properties between the top and bottom surfaces of the plate. Due to the advantageous mechanical behaviors of FG plates they are seeing increased use in a variety of engineering applications [1]. A significant number of studies have been performed to examine the mechanical behavior of FG plates see e.g., [2] for a review. It is widely accepted [2] that plate theories such as the first-order shear deformable theory (FSDT), sometimes also referred to as the Reissner-Mindlin theory, that take into account the shear-deformation effect are necessary to adequately capture the physical behavior of thick plates. Therefore the classical, or Kirchhoff plate theory, which does not capture the effect of shear deformations is not a suitable model for thick FG plates.

Historically the FSDT [3], sometimes also referred to as the Reissner-Mindlin theory, has been popular in computational mechanics for two main reasons: firstly, as mentioned above, it captures the extra physics of shear-deformation not present in the classical theory, and secondly, it relaxes the C^1 continuity requirement of the classical theory to C^0. This C^0 continuity requirement is easier to satisfy using the low-order Lagrangian finite elements that form the basis of most finite element packages. However it is well-known that naïve numerical implementations of the standard FSDT using low-order Lagrangian shape functions typically suffer from shear-locking in the thin-plate or Kirchhoff limit resulting in totally incorrect solutions. Special techniques usually based on the application of a mixed variational formulation, such as the MITC family of elements [4], solve the shear-locking problem, but with additional expense and implementation complexity.

However, with the introduction of numerical methods relying on basis functions with natural C^1 continuity such as NURBS in an isogeometric analysis framework (IGA) [5] and meshfree methods [6, 7] we believe that the physical accuracy and straightforward numerical implementation are no longer at odds. In this paper we develop a simple, efficient, and locking-free numerical method for thin through to thick shear-deformable plates by using a C^1 continuity formulation that includes the effects of shear-deformation. We prove its efficacy by studying homogeneous and functionally graded plates.

The underlying differential equation in our formulation is based on the simple FSDT (S-FSDT)

recently presented in [8, 9]. The key idea in the derivation of the S-FSDT is the decomposition of the transverse displacements in the FSDT into bending and shear parts before eliminating the rotation variables using the partial derivatives of the transverse bending displacement only. This weak formulation of the S-FSDT problem requires C^1 continuity just like in the classical plate theory but also includes the shear deformable physics of the FSDT. Therefore as well as being viewed as a simple FSDT, this formulation could also be viewed as a classical theory augmented with the shear-deformable physics of the FSDT formulation. Furthermore because the rotation variables of the standard FSDT are eliminated in terms of the bending transverse displacements the resulting weak formulation contains only four variables rather than the usual five, resulting in reduced computational expense.

In the thin-plate limit the S-FSDT recovers the classical plate theory just like the standard FSDT. However, because the thin-plate limit is included naturally in the S-FSDT formulation there is no need to resort to special numerical formulations to eliminate shear-locking as in the standard FSDT; as long as the basis functions satisfy C^1 continuity the formulation will be free from shear-locking. Other authors have also used modified plate formulations to ease the construction of numerical methods; recently, Brezzi et al. [10] introduced the twist-Kirchhoff theory that uses a partial Kirchhoff hypothesis to create a simple thin-plate finite element method. Cho and Atluri [11] use a change of variables from transverse displacement to shear stress to develop a meshfree method for the Timoshenko beam problem that is free from shear-locking. This type of approach has been extended by Tiago and Leitão [12] to the plate problem.

Because of the requirement of C^1 continuity we develop the S-FSDT within the framework of the isogeometric analysis (IGA) method proposed by Hughes et al. [5]. This method is becoming popular because of its many advantages, such as exact geometrical modeling, higher-order continuity, and simple mesh refinement. However, the primary reason for using the IGA method in this paper is to achieve the C^1 continuity condition required by the weak form of the S-FSDT. As such, other numerical methods with natural C^1 continuity such as meshfree methods [2, 6] are also be excellent candidates for the discretization of the S-FSDT.

The principle of IGA involves the adoption of CAD basis functions such as non-uniform rational B-spline (NURBS) functions as the shape functions of finite element analysis. The IGA has been successfully implemented in many engineering problems including structural vibrations [13], plates and shells [14-19], fluid mechanics [20], fluid-structure interaction problems [21], damage and

fracture mechanics[22], and structural shape optimization [23].

It is important to note that the usual IGA method also suffers from shear-locking when discretizing the standard FSDT problem, just like the standard Lagrangian finite element method. The most common remedy is to increase the polynomial order of consistency such that the basis functions are better able to represent the Kirchhoff limit. Echter and Bischoff [24] shows that this can result in sub-optimal convergence and reduce numerical efficiency in the IGA, and present a solution to the problem of shear-locking based on the Discrete Shear Gap (DSG) methodology for the 1D Timoshenko beam problem. Valizadeh et al. [14] use a modified shear correction factor dependent on the local discretization size to suppress shear locking. Beirão da Veiga et al. [25] present a method where the NURBS basis functions satisfy the Kirchhoff condition *a priori*. The resulting method is completely free of shear-locking, but requires a more complex basis function construction which involves a contravariant mapping for the basis functions interpolating the rotation variable. In contrast, the method we develop in this paper is considerably simpler and can be easily implemented using the existing functionality in open-source IGA frameworks such as igafem [26] and GeoPDEs [27].

In summary, the main objective of this study is to propose a new locking-free plate formulation for solving the static bending, buckling, and free vibration of both thin and thick FG plates. The new approach uses the high continuity of IGA to discretize the S-FSDT. The resulting S-FSDT-based IGA method has four degrees of freedom and is easy to implement within existing open-source IGA frameworks. We show the efficacy of the resulting method with extensive numerical examples focusing on functionally graded plates in static bending, free vibration, and buckling. We show the shear-locking free nature of the proposed method. The effects of boundary condition, gradient index, and geometric shape on the mechanical responses of FG plates are investigated numerically. The computed results are in typically within 1% of reference solutions in available in the literature.

The paper is structured as follows. Section 2 briefly presents the theoretical formulation. Section 3 describes NURBS-based isogeometric analysis in detail. Section 4 presents the validation of the locking-free characteristic of the proposed method. Section 5 shows the numerical results derived from the proposed IGA and in Section 6 we discuss the proposed method and suggest directions for future work.

2. Formulation

2.1. Functionally graded plate

Consider a ceramic-metal FG plate with thickness *h*. The bottom and top faces of the plate are assumed to be fully metallic and ceramic, respectively. The *xy*-plane is the mid-plane of the plate, and the positive *z*-axis is upward from the mid-plane. In this study, Poisson's ratio ν is constant and Young's modulus *E* and density ρ vary through the thickness with a power law distribution:

$$E(z) = E_m + (E_c - E_m)\left(\frac{1}{2} + \frac{z}{h}\right)^n, \tag{1}$$

$$\rho(z) = \rho_m + (\rho_c - \rho_m)\left(\frac{1}{2} + \frac{z}{h}\right)^n, \tag{2}$$

where *n* is the gradient index, *z* is the thickness coordinate variable with $-h/2 \le z \le h/2$, and subscripts *c* and *m* represent the ceramic and metal constituents, respectively.

2.2. Brief on the S-FSDT

In this subsection, we briefly present the theoretical formula of the S-FSDT. For more details, we refer the reader to [8, 9]. In the standard FSDT the three-dimensional displacement field (u,v,w) can be expressed in terms of five unknown variables as follows:

$$\begin{aligned} u(x,y,z) &= u_0(x,y) + z\phi_x(x,y) \\ v(x,y,z) &= v_0(x,y) + z\phi_y(x,y), \\ w(x,y,z) &= w_0(x,y) \end{aligned} \tag{3}$$

where u_0, v_0, and w_0 represent the displacements at the mid-plane of a plate in the *x*, *y*, and *z* directions respectively; ϕ_x and ϕ_y denote the transverse normal rotations of the *y* and *x* axes.

To derive the simple FSDT (S-FSDT), the following assumptions are made to simplify the FSDT: (a) the transverse displacement w_0 is divided into bending component w_b and shear component w_s, i.e., $w_0 = w_b + w_s$; (b) The rotation variable in the FSDT is expressed in terms of the bending component only $\phi_x = -\partial w_b / \partial x$, $\phi_y = -\partial w_b / \partial y$. Therefore, Eq. (3) can be rewritten as follows:

$$
\begin{aligned}
u(x,y,z) &= u_0(x,y) - z\partial w_b(x,y)/\partial x \\
v(x,y,z) &= v_0(x,y) - z\partial w_b(x,y)/\partial y \\
w(x,y,z) &= w_b(x,y) + w_s(x,y)
\end{aligned}
\quad . \tag{4}
$$

In contrast with the FSDT, the displacement fields in Eq. (4) for the S-FSDT contain only four unknowns, namely, u_0, v_0, w_b, w_s. Because the rotations are obtained by using the partial derivatives of the bending component w_b conforming discretizations of the S-FSDT are inherently free from the issue of shear-locking.

The three physically relevant boundary conditions for the S-FSDT are the clamped, simply supported and free conditions, as in the Kirchhoff-Love or classical plate theory. In contrast, the FSDT has five physically relevant boundary conditions, hard clamped, soft clamped, hard simply supported, soft simply supported and free. Interested readers are referred to Arnold and Falk [28] for an in-depth discussion. Although the boundary conditions in the FSDT are more descriptive than the S-FSDT, in practical terms we have not found this to be an issue as demonstrated in the results section where good agreement with the FSDT is achieved.

By making the usual small strain assumptions, the strain–displacement relations are expressed as follows:

$$
\begin{Bmatrix} \varepsilon_x \\ \varepsilon_y \\ \varepsilon_{xy} \\ \gamma_{xz} \\ \gamma_{yz} \end{Bmatrix} = \begin{Bmatrix} \dfrac{\partial u_0}{\partial x} - z\dfrac{\partial^2 w_b}{\partial x^2} \\ \dfrac{\partial v_0}{\partial y} - z\dfrac{\partial^2 w_b}{\partial y^2} \\ \dfrac{\partial u_0}{\partial y} + \dfrac{\partial v_0}{\partial x} - 2z\dfrac{\partial^2 w_b}{\partial x \partial y} \\ \dfrac{\partial w_s}{\partial x} \\ \dfrac{\partial w_s}{\partial y} \end{Bmatrix} . \tag{5}
$$

Then Eq. (5) can be written in the following matrix form:

$$
\boldsymbol{\varepsilon} = \begin{Bmatrix} \boldsymbol{\varepsilon}_0 \\ \mathbf{0} \end{Bmatrix} + \begin{Bmatrix} -z\boldsymbol{\kappa} \\ \boldsymbol{\gamma} \end{Bmatrix} , \tag{6}
$$

with

$$\boldsymbol{\varepsilon}_0 = \begin{Bmatrix} \dfrac{\partial u_0}{\partial x} \\ \dfrac{\partial v_0}{\partial y} \\ \dfrac{\partial u_0}{\partial y} + \dfrac{\partial v_0}{\partial x} \end{Bmatrix}; \quad \boldsymbol{\kappa} = \begin{Bmatrix} \dfrac{\partial^2 w_b}{\partial x^2} \\ \dfrac{\partial^2 w_b}{\partial y^2} \\ 2\dfrac{\partial^2 w_b}{\partial x \partial y} \end{Bmatrix}; \quad \boldsymbol{\gamma} = \begin{Bmatrix} \dfrac{\partial w_s}{\partial x} \\ \dfrac{\partial w_s}{\partial y} \end{Bmatrix}. \tag{7}$$

The constitutive relations are derived from Hooke's law by the following equation:

$$\boldsymbol{\sigma} = \mathbf{D}_m(z)\left(\boldsymbol{\varepsilon}_0 - z\boldsymbol{\kappa}\right) \ , \ \boldsymbol{\tau} = \mathbf{D}_s(z)\boldsymbol{\gamma}, \tag{8}$$

with

$$\boldsymbol{\sigma} = \begin{bmatrix} \sigma_x & \sigma_y & \sigma_{xy} \end{bmatrix}^T, \boldsymbol{\tau} = \begin{bmatrix} \tau_{xz} & \tau_{yz} \end{bmatrix}^T \tag{9a}$$

$$\mathbf{D}_m(z) = \frac{E(z)}{1-\nu^2}\begin{bmatrix} 1 & \nu & 0 \\ \nu & 1 & 0 \\ 0 & 0 & (1-\nu)/2 \end{bmatrix}, \tag{9b}$$

$$\mathbf{D}_s(z) = \frac{kE(z)}{2(1+\nu)}\begin{bmatrix} 1 & 0 \\ 0 & 1 \end{bmatrix} \tag{9c}$$

where k is the shear correction factor. In this paper, we set k = 5/6.

3. NURBS-based isogeometric analysis

In this section we give an overview of the NURBS basis function construction and derive the discrete weak form for the S-FSDT numerical formulation.

3.1. NURBS basis function

In 1D parametric space $\xi \in [0,1]$, a knot vector $\boldsymbol{k}(\xi)$ is a set of non-decreasing numbers that are between zero and one:

$$\boldsymbol{k}(\xi) = \left\{\xi_1 = 0, \ldots, \xi_i, \ldots, \xi_{n+p+1} = 1\right\}^T, \tag{10}$$

where i is the knot index, ξ_i is the i^{th} knot, n is the number of basis functions, and p is the order of the polynomial.

The knot vector $\boldsymbol{k}(\xi)$ is called an open knot vector when the two ends of the knot are repeated p + 1 times. Basis functions that are defined with an open knot vector are interpolatory at the beginning and end of the parametric space interval; thus, the open knot vector is used here.

By using the given knot vector $\boldsymbol{k}(\xi)$, the i^{th} B-spline basis function of degree p, written as $N_{i,p}(\xi)$, is defined recursively as follows [29]:

$$N_{i,0}(\xi)=\begin{cases}1 & if\ \xi_i \le \xi < \xi_{i+1} \\ 0 & \text{otherwise}\end{cases} \quad \text{for} \quad p=0, \tag{11}$$

and

$$N_{i,p}(\xi)=\frac{\xi-\xi_i}{\xi_{i+p}-\xi_i}N_{i,p-1}(\xi)+\frac{\xi_{i+p+1}-\xi}{\xi_{i+p+1}-\xi_{i+1}}N_{i+1,p-1}(\xi) \quad \text{for} \quad p\ge 1. \tag{12}$$

The NURBS basis function $R_{i,p}(\xi)$ in the framework of partition of unity is constructed by a weighted average of the B-spline basis functions [29]:

$$R_{i,p}(\xi)=\frac{N_{i,p}(\xi)w_i}{\sum_{j=1}^{n}N_{j,p}(\xi)w_j}, \tag{13}$$

where w_i is the i^{th} weight, and $0<w_i\le 1$.

Similarly, 2D NURBS basis functions can be constructed by taking the tensor product of two 1D B-spline basis functions as follows:

$$R_{i,j}^{p,q}(\xi,\eta)=\frac{N_{i,p}(\xi)N_{j,q}(\eta)w_{i,j}}{\sum_{i=1}^{n}\sum_{j=1}^{m}N_{i,p}(\xi)N_{j,q}(\eta)w_{i,j}}, \tag{14}$$

where $w_{i,j}$ represents the 2D weight; $N_{i,p}(\xi)$ and $N_{j,q}(\eta)$ are the B-spline basis functions of order p in the ξ direction and order q in the η direction, respectively; $N_{j,q}(\eta)$ follows the recursive formula shown in Eqs. (11) and (12) with knot vector $\boldsymbol{k}(\eta)$. The definition of $\boldsymbol{k}(\eta)$ is similar to that of $\boldsymbol{k}(\xi)$.

By using the NURBS basis functions, a NURBS surface of order p in the ξ direction and order q in the η direction can be constructed as follows:

$$\boldsymbol{S}(\xi,\eta)=\sum_{i=1}^{n}\sum_{j=1}^{m}R_{i,j}^{p,q}(\xi,\eta)\boldsymbol{B}_{i,j}, \tag{15}$$

where $\boldsymbol{B}_{i,j}$ represents the coordinates of control points in two dimensions.

3.2. Discrete equations

The parametric domain in IGA is similar to the isoparametric space in the finite element method (FEM). Thus, the generalized displacements in the middle plane are approximated as follows:

$$\mathbf{u}_0^h = \sum_{I=1}^{NP} R_I \mathbf{u}_I \quad , \tag{16}$$

with

$$\mathbf{u}_0^h = \begin{bmatrix} u_0^h & v_0^h & w_b^h & w_s^h \end{bmatrix}^T , \tag{17a}$$

$$\mathbf{u}_I = \begin{bmatrix} u_I & v_I & w_{bI} & w_{sI} \end{bmatrix}^T . \tag{17b}$$

where $NP = (p+1)(q+1)$ is the number of control points per element, and R_I and $\mathbf{u}_I$ denote the shape function and the unknown displacement vector at control point I, respectively.

By substituting Eq. (16) into Eq. (7), one can obtain the following:

$$\boldsymbol{\varepsilon}_0 = \sum_{I=1}^{NP} \mathbf{B}_I^m \mathbf{u}_I \quad , \quad \boldsymbol{\kappa} = \sum_{I=1}^{NP} \mathbf{B}_I^b \mathbf{u}_I \quad , \quad \boldsymbol{\gamma} = \sum_{I=1}^{NP} \mathbf{B}_I^s \mathbf{u}_I , \tag{18}$$

with

$$\mathbf{B}_I^m = \begin{bmatrix} R_{I,x} & 0 & 0 & 0 \\ 0 & R_{I,y} & 0 & 0 \\ R_{I,y} & R_{I,x} & 0 & 0 \end{bmatrix}, \mathbf{B}_I^b = \begin{bmatrix} 0 & 0 & R_{I,xx} & 0 \\ 0 & 0 & R_{I,yy} & 0 \\ 0 & 0 & 2R_{I,xy} & 0 \end{bmatrix}, \mathbf{B}_I^s = \begin{bmatrix} 0 & 0 & 0 & R_{I,x} \\ 0 & 0 & 0 & R_{I,y} \end{bmatrix}, \tag{19}$$

For the static problem, the weak form can be expressed as follows:

$$\int_\Omega \delta\boldsymbol{\varepsilon}^T \mathbf{D} \boldsymbol{\varepsilon} d\Omega + \int_\Omega \delta\boldsymbol{\gamma}^T \mathbf{D}^s \boldsymbol{\gamma} d\Omega = \int_\Omega \delta\left(w_b + w_s\right) f d\Omega , \tag{20}$$

where f is the transverse loading per unit area and

$$\boldsymbol{\varepsilon} = \begin{bmatrix} \boldsymbol{\varepsilon}_0 \\ \boldsymbol{\kappa} \end{bmatrix}, \mathbf{D} = \begin{bmatrix} \mathbf{D}^m & \overline{\mathbf{B}} \\ \overline{\mathbf{B}} & \mathbf{D}^b \end{bmatrix}, \mathbf{D}^s = \int_{-h/2}^{h/2} \mathbf{D}_s(z)\, dz , \tag{21}$$

with

$$\mathbf{D}^m = \int_{-h/2}^{h/2} \mathbf{D}_m(z)\, dz , \quad \overline{\mathbf{B}} = \int_{-h/2}^{h/2} z\mathbf{D}_m(z)\, dz , \quad \mathbf{D}^b = \int_{-h/2}^{h/2} z^2 \mathbf{D}_m(z)\, dz . \tag{22}$$

For the free vibration analysis, a weak form can be expressed as follows:

$$\int_\Omega \delta\boldsymbol{\varepsilon}^T \mathbf{D} \boldsymbol{\varepsilon} d\Omega + \int_\Omega \delta\boldsymbol{\varepsilon}^T \mathbf{D}^s \boldsymbol{\varepsilon} d\Omega = \int_\Omega \delta\mathbf{u}^T \mathbf{m} \ddot{\mathbf{u}} d\Omega , \tag{23}$$

where

$$\mathbf{m} = \begin{bmatrix} I_0 & I_1 \\ I_1 & I_2 \end{bmatrix}, \quad (I_0, I_1, I_2) = \int_{-h/2}^{h/2} \rho(z)(1, z, z^2) dz , \tag{24}$$

$$\mathbf{u}=\begin{bmatrix}\mathbf{u}_1\\ \mathbf{u}_2\end{bmatrix},\mathbf{u}_1=\begin{Bmatrix}u_0^h\\ v_0^h\\ w_b^h+w_s^h\end{Bmatrix}=\sum_{I=1}^{NP}\mathbf{N}_I^1\mathbf{u}_I\,,\mathbf{u}_2=\begin{Bmatrix}\partial w_b^h/\partial x\\ \partial w_b^h/\partial y\\ 0\end{Bmatrix}=\sum_{I=1}^{NP}\mathbf{N}_I^2\mathbf{u}_I\,, \tag{25}$$

with

$$\mathbf{N}_I^1=\begin{bmatrix}R_I & 0 & 0 & 0\\ 0 & R_I & 0 & 0\\ 0 & 0 & R_I & R_I\end{bmatrix}\,,\ \mathbf{N}_I^2=\begin{bmatrix}0 & 0 & R_{I,x} & 0\\ 0 & 0 & R_{I,y} & 0\\ 0 & 0 & 0 & 0\end{bmatrix}. \tag{26}$$

Finally, for the buckling analysis, the weak form can be expressed as follows:

$$\int_\Omega\delta\boldsymbol{\varepsilon}^T\mathbf{D}\boldsymbol{\varepsilon}d\Omega+\int_\Omega\delta\boldsymbol{\gamma}^T\mathbf{D}^s\boldsymbol{\gamma}d\Omega+\int_\Omega\nabla^T\delta\left(w_b+w_s\right)\hat{\boldsymbol{\sigma}}_0\nabla\left(w_b+w_s\right)d\Omega=0\,. \tag{27}$$

where $\nabla^T=\left[\partial/\partial x\quad\partial/\partial y\right]^T$ is the gradient operator and $\hat{\boldsymbol{\sigma}}_0=\begin{bmatrix}\sigma_x^0 & \tau_{xy}^0\\ \tau_{xy}^0 & \sigma_y^0\end{bmatrix}$ is the pre-buckling stresses under the in-plane.

By substituting Eqs. (18) and (21) into Eqs. (20), (23), and (27), the formulations of the static, free vibration, and buckling problems are rewritten in the following form:

$$\mathbf{Kd}=\mathbf{F}\,, \tag{28}$$

$$\left(\mathbf{K}-\omega^2\mathbf{M}\right)\mathbf{d}=0\,, \tag{29}$$

$$\left(\mathbf{K}-\lambda_{cr}\mathbf{K}_g\right)\mathbf{d}=0\,, \tag{30}$$

where the global stiffness matrix $\mathbf{K}$ is given by the following:

$$\mathbf{K}=\int_\Omega\begin{Bmatrix}\mathbf{B}^m\\ \mathbf{B}^b\end{Bmatrix}^T\begin{bmatrix}\mathbf{D}^m & \overline{\mathbf{B}}\\ \overline{\mathbf{B}} & \mathbf{D}^b\end{bmatrix}\begin{Bmatrix}\mathbf{B}^m\\ \mathbf{B}^b\end{Bmatrix}d\Omega+\int_\Omega\left(\mathbf{B}^s\right)^T\mathbf{D}^s\mathbf{B}^s d\Omega\,. \tag{31}$$

The load vector $\mathbf{F}$ is computed as follows:

$$\mathbf{F}=\int_\Omega f\mathbf{N}d\Omega,\ \text{and}\ \mathbf{N}_I=\begin{bmatrix}0 & 0 & R_I & R_I\end{bmatrix}^T. \tag{32}$$

The global mass matrix $\mathbf{M}$ is expressed as follows:

$$\mathbf{M}=\int_\Omega\begin{Bmatrix}\mathbf{N}^1\\ \mathbf{N}^2\end{Bmatrix}^T\mathbf{m}\begin{Bmatrix}\mathbf{N}^1\\ \mathbf{N}^2\end{Bmatrix}d\Omega\,. \tag{33}$$

The geometric stiffness matrix $\mathbf{K}_g$ is expressed as follows:

$$\mathbf{K}_g=\int_\Omega\left(\mathbf{B}^g\right)^T\hat{\boldsymbol{\sigma}}_0\mathbf{B}^g d\Omega\,, \tag{34}$$

with

$$\mathbf{B}_I^g = \begin{bmatrix} 0 & 0 & R_{I,x} & R_{I,x} \\ 0 & 0 & R_{I,y} & R_{I,y} \end{bmatrix}. \tag{35}$$

4. Validation of the fully locking-free property

A homogeneous square plate with length a and thickness h under a uniform load P = 1N is considered to test the locking-free characteristic of the developed approach. The material parameters used for this particular study are Young's modulus E = 1.092 × 10^6 N/mm^2 and Poisson's ratio ν = 0.3. The simply supported and clamped boundary conditions are considered. The rotations are obtained by using the derivatives of bending deflection $\phi_x = -\partial w_b / \partial x$ and $\phi_y = -\partial w_b / \partial y$; thus, the constraint on the rotations in the clamped boundary condition is imposed by fixing the z-component of the second row of control points as in [17]. The central deflection is normalized by $\overline{w} = \dfrac{100 w_c E h^3}{12\left(1-\nu^2\right) P a^4}$.

Quadratic and cubic NURBS basis functions are used in this study. The control points and physical mesh for the cubic NURBS basis function are shown in Fig. 1. The computed results of the normalized central deflections obtained using the IGA based on both the S-FSDT and original FSDT are compared with the analytical solutions [30] (Table 1). Some interesting issues may be observed from the results:

1. the FSDT-based IGA suffers shear locking when the length–thickness ratio a/h is greater than 100 for the quadratic NURBS basis functions and a/h is greater than 1000 for the cubic NURBS basis functions. We conclude that increasing the polynomial order is not sufficient to completely eliminate shear-locking when using the FSDT-based IGA.
2. the S-FSDT-based IGA is completely free from shear-locking when using both quadratic and cubic NURBS basis functions; therefore our S-FSDT-based IGA based method guarantees shear-locking free results, unlike the FSDT-based IGA method.
3. Increasing the polynomial order of the basis functions increases the accuracy of the proposed S-FSDT IGA method.

We also verify that the S-FSDT converges to the values given by the FSDT for thick plates and Kirchhoff–Love theory for thin plates. The normalized central deflections, bending deflections

$\bar{w}_b = \frac{100 w_b E h^3}{12\left(1-\nu^2\right) P a^4}$, and shear deflections $\bar{w}_s = \frac{100 w_s E h^3}{12\left(1-\nu^2\right) P a^4}$ obtained by the IGA based on the S-FSDT with different length–thickness ratios *a*/*h* are show in Table 2. Table 2 shows the following: (1) when *a*/*h* < 20, the shear deformation effects are considered in S-FSDT, similar to FSDT; (2) the effects of the shear component decreases with increasing *a*/*h*; (3) when *a*/*h* > 20, the effects of shear component are negligible, and the S-FSDT converges to the value given by the Kirchhoff-Love theory.

5. Numerical applications

In this section, the static bending, free vibration, and buckling behavior of homogeneous and FG plates with different geometric shapes are examined by using the developed "*S-FSDT-based IGA*" model with cubic NURBS basis function. A 4 × 4 Gaussian quadrature scheme is used in each NURBS element to integrate the weak form. An original "*FSDT-based IGA*" computer code is implemented to the same problems for comparison purposes. In the following examples, the boundaries of the plate are denoted as simply supported (S), clamped (C), and free (F). A mesh of 16 × 16 control points is used for the square plates unless stated otherwise.

5.1. Static analysis

5.1.1. Convergence and accuracy study

To validate the convergence of the S-FSDT-based IGA, a fully simply supported Al/Al_2O_3 square plate with a length–thickness ratio of *a*/*h* = 100 and different gradient indexes *n* under sinusoidal loads $P\sin(\pi x)\sin(\pi y)$ is considered. The material properties of Al are ν_m=0.3, E_m=70*GPa*, and ρ_m=2707kg/m^3, and the material properties of Al_2O_3 are ν_c=0.3, E_c=380*GPa*, ρ_c=3800kg/m^3. The central deflection is normalized by $\bar{w} = 10 w_c E_c h^3 / (Pa^4)$. Table 3 presents the comparison of the normalized central deflections derived from the S-FSDT-based IGA, the FSDT-based IGA, and the analytical solutions [8, 31, 32]. The numerical results in the convergence study of the relative error of normalized central deflection $\left|\frac{\bar{w}-\bar{w}_{\text{exact}}}{\bar{w}_{\text{exact}}}\right|$ are shown in Fig. 2, and the analytical solutions based on S-FSDT [8] are adopted. Table 3 shows that the results obtained with

S-FSDT are similar to the analytical solutions and match well with the results derived from the FSDT-based IGA. The amplitude of the normalized central deflections increases with increasing values of the gradient index.

Another example is performed to illustrate the accuracy of the developed approach. In this example, the conditions are the same as the previous example except for the length–thickness ratio *a*/*h*. Table 4 shows the normalized central deflections obtained with the S-FSDT-based IGA, the FSDT-based IGA, and the analytical solutions [8, 31, 32]. The results from the present method are in good agreement with the analytical solutions [8, 31, 32] for both thin and thick plates, thus confirming the accuracy of the proposed approach.

5.1.2. Bending analysis

In this subsection the bending behavior of square and circular FG plates is investigated.

5.1.2.1. Square plate

An Al/ZrO_2-1 square plate with different boundary conditions, length-thickness ratios *a*/*h*, and gradient indexes *n* under a uniform load is analyzed. The material properties of Al are v_m=0.3 and E_m=70GPa and those of ZrO_2-1 are v_c=0.3 and E_c=200GPa. The central deflection is normalized by $\bar{w} = \frac{100 w_c E_m h^3}{12\left(1-v_m^2\right) P a^4}$. Table 5 shows the normalized central deflections obtained with the S-FSDT-based IGA, FSDT-based IGA, FSDT-based kp-Ritz method [33], and FSDT-based edge-based smoothed FEM [34]. The results obtained with the S-FSDT-based IGA match well with those derived from other techniques. For all boundary conditions and length–thickness ratios, remarkable agreements are achieved between the S-FSDT-based IGA and FSDT-based IGA techniques. When the boundary condition changes from SSSS to SFSS and SFSF, the structural stiffness is gradually reduced; thus, the deflection magnitude is gradually increased. The deflection magnitude is increased by increasing the gradient index *n*.

To further examine the effect of the boundary conditions and gradient index on the central deflection of the FG plate, an Al/Al_2O_3 thin plate with a length–thickness ratio of *a*/*h* = 100 under a uniform load P is considered. The central deflection is normalized by $\bar{w} = \frac{10 w_c E_c h^3}{P a^4}$. The normalized central deflections obtained by the S-FSDT-based IGA and FSDT-based IGA are

presented in Table 6. The S-FSDT and FSDT deliver a similar result for all boundary conditions and gradient indices. A similar phenomenon to that of the Al/ZrO_2-1 plate is observed, i.e., when the boundary condition changes from CCCC and SCSC to SSSS and SFSF, the magnitude of the deflection is gradually increased. Fig. 3 shows the shapes of transverse displacement for the various boundary conditions and gradient index n = 2.

5.1.2.2 Circular plate

To demonstrate the applicability of the present method to model common engineering shapes, the bending behavior of circular plate is studied in this subsection.

First, a homogeneous circular plate with thickness h = 0.01 m and radius R = 1 m subjected to a uniform transverse pressure P = 100 N is considered. Two different boundary conditions are considered: fully simply supported and fully clamped on the entire edges. The material properties of the plate are $E = 1.092 \times 10^6$ N/m^2 and ν = 0.3. Fig. 4 shows the mesh of 121 control points. The central deflection is normalized by $\bar{w} = \frac{w_c E h^3}{P R^4 12(1-\nu^2)}$. The comparisons between the normalized central deflections obtained with the S-FSDT-based IGA, FSDT-based IGA, analytical solutions [35], and Kirchhoff theory-based MLPG [35] are listed in Table 7. The obtained results from the developed method are in good agreement with the analytical and MLPG solutions.

We then investigate the bending behavior of titanium/zirconium circular plate with different *h/R* under roller supported and clamped boundary conditions subjected to a uniform pressure on the top surface of the plate. The material properties of titanium are ν_m=0.288 and E_m=110.25GPa and those of zirconium are ν_c=0.288 and E_c=278.41GPa. The deflection shapes of the plates are plotted in Fig. 5. Table 8 shows the normalized deflection $\bar{w} = \frac{64 w_c E h^3}{12\left(1-\nu^2\right) P R^4}$ at the center of the plate. A good agreement with HSDT based IGA [15], elasticity solutions [36] and semi-analytical numerical method [37] is obtained. A similar deflection pattern to that of the square plate is observed.

5.2. Free vibration

5.2.1. Square plate

A fully simply supported Al/Al_2O_3 square plate with different length–thickness ratios *a/h* is analyzed. The obtained results of the first normalized natural frequencies $\omega^* = \omega h\sqrt{\rho_c / E_c}$ with meshes of 6, 8, 12, 16, and 24 control points per side are listed in Table 9, which shows fast the convergence of the results. The first normalized natural frequencies $\omega^* = \omega h\sqrt{\rho_c / E_c}$ obtained with different methods for several specified gradient indices are listed in Table 10. A good agreement among the obtained results with other reference solutions is evident, e.g., the magnitude of natural frequency decreases with increasing length–thickness ratios *a/h*. The reference solutions are taken from the analytical methods with high order and third shear deformation theories [38, 39], FEM with the S-FSDT [40], and element-free kp-Ritz method with FSDT [41] (Table 10). The model analysis shows that the amplitude of the first normalized natural frequency increases with the increasing value of the gradient index, similar to static bending.

To investigate the effects of the boundary conditions on the natural frequency, an Al/Al_2O_3 square thin plate with a length–thickness ratio of *a/h* = 100 under different boundary conditions and gradient indexes is considered. The first five mode normalized natural frequencies $\omega^* = \omega\pi^2\left(a^2/h\right)\sqrt{\rho_m / E_m}$ obtained with different methods are listed in Table 11. The results obtained with the S-FSDT-based IGA are in good agreement with the results from the FSDT-based IGA, CPT-neu-based IGA [42], and analytical solutions [43]. When the boundary conditions change from CCCC to SCSC, SSSS, and SFSF, the magnitude of the natural frequency gradually decreases. The magnitude of the natural frequency decreases with an increasing gradient index.

The first six mode shapes of fully simply supported and fully clamped square Al/Al_2O_3 thin plates with a length–thickness ratio of *a/h* =100 and a gradient index of *n* = 2 are given in Figs. 6 and 7, respectively.

5.2.2. Circular plate

We consider a clamped Al/Al_2O_3 circular plate with different thickness–radius ratios *h*/*R*. The frequency is normalized by $\omega^* = 100\omega h\sqrt{\rho_c / E_c}$. The obtained results shown in Table 12 agree with the results obtained by the FSDT-based IGA, HSDT-based IGA [15], FSDT-based semi-analytical solutions [44], FEM with ABAQUS, and uncoupled model (UM) with FSDT proposed by Ebrahimi et al.[45]. Decreasing the length–thickness ratio h/R increases the magnitude

of the natural frequency. The first six mode shapes of the circular plate are plotted in Fig. 8.

The first normalized frequencies $\omega^* = 100\omega h\sqrt{\rho_c / E_c}$ of the Al/Al_2O_3 circular plate with different boundary conditions and gradient indexes *n* are tested and shown in Table 13. The magnitude of natural frequency decreases with an increasing gradient index. The natural frequencies of free and simply supported plates are lower than that of the clamped boundary plate.

5.2.3. Square plate with a complicated cutout

To illustrate the applicability of the proposed method for realistic geometries, a thin homogenous square plate with a complicated cutout is considered (Fig. 9). The material and geometrical parameters are Young's modulus E = 200 × 10^9 Pa, Poisson's ratio ν = 0.3, mass density ρ = 8,000 kg/m^3, and thickness h = 0.05 m. The plate consists of 8 NURBS patches (as depicted in Figure 9), and 392 control points with 160 elements are considered (Fig. 10). Given that C^1 continuity is required in the S-FSDT, the bending strip method proposed by Kiendl et al. [46] is applied to maintain C^1 continuity between patches. The stiffness of the bending strip stiffness is set as E_s = 10^8 Pa in this paper. The normalized natural frequency $\omega^* = \left(\omega^2 \rho h a^4 / D\right)^4$ results obtained by the proposed method are listed in Table 14 for simply supported and clamped boundary condition, where $D = Eh^3 / \left(12\left(1-\nu\right)\right)$ is the flexural rigidity of the plates. In addition to the FSDT-based IGA results, some available results obtained by Kirchhoff on the IGA [47], MKI method [48], EFG method [49], and node-based smoothing RPIM (NS-RPIM) method [50] are also presented for comparison purposes. The S-FSDT-based IGA results are in good agreement with the reference solutions for all considered boundary conditions.

5.3. Buckling analysis

The buckling load of a homogeneous rectangular plate with length a, width b, and thickness h is computed. The pre-buckling forces can be obtained by using the equilibrium conditions expressed as follows:

$$\sigma_x^0 = \varsigma_1 P_1, \quad \sigma_y^0 = \varsigma_2 P_1, \quad \tau_{xy}^0 = 0, \tag{36}$$

where P_1 is the force per unit length, and ς_1 and ς_2 are the load parameters that indicate the loading conditions. Negative values indicate that the plate is subjected to biaxial compressive loads, whereas positive values are used for tensile loads (Fig. 11).

The buckling load is normalized with $\overline{N}_{cr} = \frac{12N_{cr}a^2(1-\nu^2)}{Eh^3}$. Table 15 presents the normalized buckling loads for the homogeneous rectangular plate with different boundary conditions and aspect ratios. The results obtained by the S-FSDT-based IGA are in excellent agreement with the Levy solutions based on Kirchhoff theory [51, 52].

We also study the buckling response of an Al /Al_2O_3 plate with different boundary conditions and aspect ratios. In this study, we set *b/h* = 0.01. The buckling load (*MN/m*) is presented in Table 16 for an Al /Al_2O_3 plate with different boundary conditions and some gradient indexes. The results derived from the proposed method are in good agreement with the Levy solutions based on Kirchhoff theory [52]. Increasing the gradient index decreases the buckling load. The buckling load is increased from SFSF to SSSS and SCSC.

5. Conclusions

We presented a new locking-free plate formulation by using the characteristics of the NURBS-based IGA in combination with the S-FSDT theory for the study of homogeneous and nonhomogeneous functionally graded plates. Numerical examples for static bending, buckling and free vibration analysis were considered and their results were presented and discussed in detail. Aspects of the boundary conditions, gradient index, and geometric shape were also investigated. Our conclusions are as follows:

- the approach can be applied to thick and thin plates without special numerical techniques.
- one unknown is saved compared with the FSDT.
- the higher-order continuity of the IGA means that the potentially awkward C^1-continuity required by the S-FSDT can be satisfied easily.
- the geometry can be described exactly, and arbitrary order continuity can be achieved, due to the inherent properties of the IGA framework.
- the new method can be implemented by researchers within existing open-source IGA codes with very little effort.

We find that the S-FSDT-based IGA is well suited to the analysis of functionally graded plates. The results show the robustness and accuracy of the S-FSDT-based IGA for both thin and thick plates. In this study we focused on the linear analysis of FGM plates. However, the method we propose is general; thus, it can be extended to other problems such as nonlinear analysis of plates. We also restricted our numerical study to the relatively simple geometries such as square, rectangular, circular, and multi-patch plates in order to compare with other authors, but in combination with techniques such as trimmed surfaces [53] or the finite cell method [54], the method proposed here could be extended to highly complex structures.

Acknowledgements

This work was supported by Jiangsu Province Graduate Students Research and Innovation Plan (Grant No. CXZZ13_0235) and the National Natural Science Foundation of China (Grant No. 51179063). Jack S. Hale was supported by the Fonds National de la Recherche, Luxembourg under the AFR Marie Curie COFUND scheme and partially supported by the University of Luxembourg. Tinh Quoc Bui (ID No. P14055) was supported by the Grant-in-Aid for Scientific Research (No. 26-04055) - Japan Society for Promotion of Science (JSPS). Stephane P. A. Bordas was partially supported by the European Research Council Starting Independent Research Grant (ERC Stg grant agreement No. 279578) entitled “Towards real time multiscale simulation of cutting in non-linear materials with applications to surgical simulation and computer guided surgery”.

References

[1] Jha DK, Kant T, Singh RK. A critical review of recent research on functionally graded plates. Compos Struct 2013;96:833-849.

[2] Liew KM, Zhao X, Ferreira AJM. A review of meshless methods for laminated and functionally graded plates and shells. Compos Struct 2011;93(8):2031-2041.

[3] Reissner E. The effect of transverse shear deformation on the bending of elastic plates. J. Appl. Mech 1945; 12, A69.

[4] Bathe KJ, Brezzi F, Cho SW. The MITC7 and MITC9 Plate bending elements. Comput Struct 1989;32(3-4):797-814.

[5] Hughes TJR, Cottrell JA, Bazilevs Y. Isogeometric analysis: CAD, finite elements, NURBS, exact geometry and mesh refinement. Comput Methods Appl Mech Eng 2005;194(39-41):4135-4195.

[6] Krysl P, Belytschko T. Analysis of thin plates by the element-free Galerkin method. Comput Mech 1995;17(1-2):26-35.

[7] Neves AMA, Ferreira AJM, Carrera E, Cinefra M, Roque CMC, Jorge RMN, Soares CMM. Static, free vibration and buckling analysis of isotropic and sandwich functionally graded plates using a quasi-3D higher-order shear deformation theory and a meshless technique. Compos Part B: Eng 2013;44(1):657-674.

[8] Thai HT, Choi DH. A simple first-order shear deformation theory for the bending and free vibration analysis of functionally graded plates. Compos Struct 2013;101:332-340.

[9] Thai HT, Choi DH. A simple first-order shear deformation theory for laminated composite plates. Compos Struct 2013;106:754-763.

[10] Brezzi F, Evans JA, Hughes TJR, Marini LD. New rectangular plate elements based on twist-Kirchhoff theory. Comput Methods Appl Mech Eng 2011;200(33-36):2547-2561.

[11] Cho JY, Atluri SN. Analysis of shear flexible beams, using the meshless local Petrov-Galerkin method, based on a locking-free formulation. Eng Computation. 2001;18(1/2):215-240.

[12] Tiago C, Leitao VMA. Eliminating shear-locking in meshless methods: a critical overview and a new framework for structural theories. In: Leitao VMA, Alves C, Armando Duarte C, editors. Advances in meshfree techniques. Computational methods in applied sciences, vol. 5. Berlin:

Springer; 2007. p. 123–45.

[13] Cottrell JA, Reali A, Bazilevs Y, Hughes TJR. Isogeometric analysis of structural vibrations. Comput Methods Appl Mech Eng 2006;195(41-43):5257-5296.

[14] Valizadeh N, Natarajan S, Gonzalez-Estrada OA, Rabczuk T, Bui TQ, Bordas SPA. NURBS-based finite element analysis of functionally graded plates: Static bending, vibration, buckling and flutter. Compos Struct 2013;99:309-326.

[15] Tran LV, Ferreira AJM, Nguyen-Xuan H. Isogeometric analysis of functionally graded plates using higher-order shear deformation theory. Compos Part B: Eng 2013;51:368-383.

[16] Valizadeh N, Bui TQ, Vu VT, Thai HT, Nguyen MN. isogeometric simulation for buckling, free and forced vibration of orthotropic plates. Int. J. Appl. Mechanics 2013;05(02):1350017.

[17] Kiendl J, Bletzinger KU, Linhard J, Wüchner R. Isogeometric shell analysis with Kirchhoff–Love elements. Comput Methods Appl Mech Eng 2009;198(49-52):3902-3914.

[18] Benson DJ, Bazilevs Y, Hsu MC, Hughes TJR. Isogeometric shell analysis: The Reissner–Mindlin shell. Comput Methods Appl Mech Eng 2010;199(5-8):276-289.

[19] Shojaee S, Valizadeh N, Izadpanah E, Bui TQ, Vu TV. Free vibration and buckling analysis of laminated composite plates using the NURBS-based isogeometric finite element method. Compos Struct 2012;94(5):1677-1693.

[20] Bazilevs Y, Calo VM, Cottrell JA, Hughes TJR, Reali A, Scovazzi G. Variational multiscale residual-based turbulence modeling for large eddy simulation of incompressible flows. Comput Methods Appl Mech Eng 2007;197(1-4):173-201.

[21] Bazilevs Y, Calo VM, Hughes TJR, Zhang Y. Isogeometric fluid-structure interaction: theory, algorithms, and computations. Comput Mech 2008;43(1):3-37.

[22] Verhoosel CV, Scott MA, Hughes TJR, de Borst R. An isogeometric analysis approach to gradient damage models. Int J Numer Meth Eng 2011;86(1):115-134.

[23] Wall WA, Frenzel MA, Cyron C. Isogeometric structural shape optimization. Comput Methods Appl Mech Eng 2008;197(33-40):2976-2988.

[24] Echter R, Bischoff M. Numerical efficiency, locking and unlocking of NURBS finite elements. Comput Methods Appl Mech Eng 2010;199(5-8):374-382.

[25] da Veiga LB, Buffa A, Lovadina C, Martinelli M, Sangalli G. An isogeometric method for the Reissner–Mindlin plate bending problem. Comput Methods Appl Mech Eng 2012;209–212:45–53.

[26] Nguyen VP, Bordas SPA, Rabczuk T. Isogeometric analysis: an overview and computer implementation aspects. arXiv:1205.2129 [cs, math] (2012). at <http://arxiv.org/abs/1205.2129>.

[27] de Falco C, Reali A, Vázquez R. GeoPDEs: A research tool for Isogeometric Analysis of PDEs. Adv Eng Softw 2011;42(12):1020-1034.

[28] Arnold D, Falk R. The Boundary Layer for the Reissner–Mindlin Plate Model. Siam J Math Anal 1990;21(2):281-312.

[29] Piegl L, Tiller W. The NURBS Book. Springer Berlin Heidelberg, 1995.

[30] Zienkiewicz OC, Xu Z, Zeng LF, Samuelsson A, Wiberg N. Linked interpolation for Reissner-Mindlin plate elements: Part I—A simple quadrilateral. Int J Numer Meth Eng 1993;36(18):3043-3056.

[31] Neves AMA, Ferreira AJM, Carrera E, Cinefra M, Roque CMC, Jorge RMN, Soares CMM. A quasi-3D hyperbolic shear deformation theory for the static and free vibration analysis of functionally graded plates. Compos Struct 2012;94(5):1814-1825.

[32] Carrera E, Brischetto S, Cinefra M, Soave M. Effects of thickness stretching in functionally graded plates and shells. Compos Part B: Eng 2011;42(2):123-133.

[33] Lee YY, Zhao X, Liew KM. Thermoelastic analysis of functionally graded plates using the element-free kp-Ritz method. Smart Mater. Struct 2009;18(3):35007.

[34] Nguyen-Xuan H, Tran LV, Nguyen-Thoi T, Vu-Do HC. Analysis of functionally graded plates using an edge-based smoothed finite element method. Compos Struct 2011;93(11):3019-3039.

[35] Liu GR. Mesh free methods: moving beyond the finite element method. CRC Press, 2003.

[36] Li XY, Ding HJ, Chen WQ. Elasticity solutions for a transversely isotropic functionally graded circular plate subject to an axisymmetric transverse load qrk. Int J Solids Struct 2008;45(1):191-210.

[37] Reddy JN, Wang CM, Kitipornchai S. Axisymmetric bending of functionally graded circular and annular plates. Euro J Mechan A/Solids 1999;18(2):185-199.

[38] Matsunaga H. Free vibration and stability of functionally graded plates according to a 2-D higher-order deformation theory. Compos Struct 2008;82(4):499-512.

[39] Thai HT, Kim SE. A simple higher-order shear deformation theory for bending and free vibration analysis of functionally graded plates. Compos Struct 2013;96:165-173.

[40] Thai HT, Choi DH. Finite element formulation of various four unknown shear deformation

theories for functionally graded plates. Finite Elem Anal Des 2013;75:50-61.

[41] Zhao X, Lee YY, Liew KM. Free vibration analysis of functionally graded plates using the element-free kp-Ritz method. J Sound Vib 2009;319(3-5):918-939.

[42] Yin SH, Yu TT, Liu P. Free Vibration Analyses of FGM Thin Plates by Isogeometric Analysis Based on Classical Plate Theory and Physical Neutral Surface. Advances in Mechanical Engineering 2013;Volume 2013, Article ID 634584, 10 pages.

[43] Baferani AH, Saidi AR, Jomehzadeh E. An exact solution for free vibration of thin functionally graded rectangular plates. Proc Inst Mech Eng Part C J Mech Eng Sci 2011;225:(C3):526-536.

[44] Hosseini-Hashemi S, Fadaee M, Es'Haghi M. A novel approach for in-plane/out-of-plane frequency analysis of functionally graded circular/annular plates. Int J Mech Sci 2010;52(8):1025-1035.

[45] Ebrahimi F, Rastgoo A, Atai AA. A theoretical analysis of smart moderately thick shear deformable annular functionally graded plate. Euro J Mechan A/Solids 2009;28(5):962-973.

[46] Kiendl J, Bazilevs Y, Hsu MC, Wüchner R, Bletzinger KU. The bending strip method for isogeometric analysis of Kirchhoff–Love shell structures comprised of multiple patches. Comput Methods Appl Mech Eng 2010;199(37-40):2403-2416.

[47] Shojaee S, Izadpanah E, Valizadeh N, Kiendl J. Free vibration analysis of thin plates by using a NURBS-based isogeometric approach. Finite Elem Anal Des 2012;61:23-34.

[48] Bui TQ, Nguyen MN. A moving Kriging interpolation-based meshfree method for free vibration analysis of Kirchhoff plates. Comput Struct 2011;89(3-4):380-394.

[49] Liu GR, Chen XL. A mesh-free method for static and free vibration analyses of thin plates of complicated shape. J Sound Vib 2001;241(5):839-855.

[50] Cui XY, Liu GR, Li GY, Zhang GY. A thin plate formulation without rotation DOFs based on the radial point interpolation method and triangular cells. Int J Numer Meth Eng 2011;85(8):958-986.

[51] Yu LH, Wang CY. Buckling of rectangular plates on an elastic foundation using the Levy method. AIAA J 2008;46(12):3163–6.

[52] Mohammadi M, Saidi A, Jomehzadeh E. Levy Solution for Buckling Analysis of Functionally Graded Rectangular Plates. Appl Compos Mater 2010;17(2):81-93.

[53] Kim HJ, Seo YD, Youn SK. Isogeometric analysis for trimmed CAD surfaces. Comput Methods Appl Mech Eng 2009;198(37-40):2982-2995.

[54] Schillinger D, Ruess M, Zander N, Bazilevs Y, Düster A, Rank E. Small and large deformation analysis with the p- and B-spline versions of the Finite Cell Method. Comput Mech 2012;50(4):445-478.

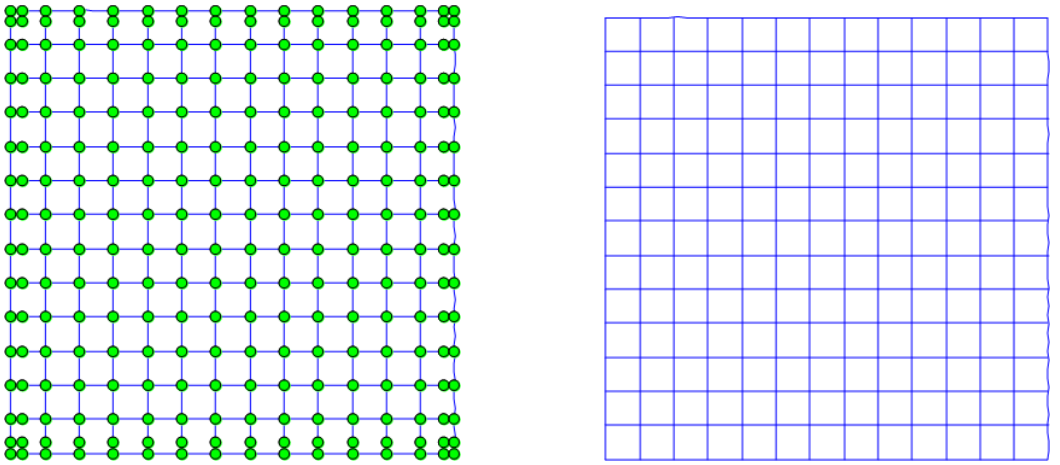

Fig. 1. A square plate with 16 × 16 control points and 13 × 13 elements by using cubic NURBS basis function: (a) control mesh and (b) physical mesh.

Table 1. Comparisons of the normalized central deflection obtained by the IGA for the S-FSDT, FSDT, and analytical method [30].

(a) Fully simply supported

a/h	Method	$\bar{w}$	Error (%)	a/h	Method	$\bar{w}$	Error (%)
20	FSDT-Quadratic	0.4114	0.1461	100	FSDT -Quadratic	**0.4048**	0.3937
	S-FSDT-Quadratic	0.4109	0.0243		S-FSDT-Quadratic	0.4058	0.1476
	FSDT-Cubic	0.4115	0.1704		FSDT-Cubic	0.4064	0
	S-FSDT-Cubic	0.4115	0.1704		S-FSDT-Cubic	0.4064	0
	Exact [30]	0.4108			Exact [30]	0.4064	
10^3	FSDT-Quadratic	0.3654	10.0443	10^4	FSDT-Quadratic	0.3552	12.5554
	S-FSDT-Quadratic	0.4056	0.1477		S-FSDT-Quadratic	0.4056	0.1477
	FSDT-Cubic	**0.4069**	0.1723		FSDT-Cubic	0.3825	5.8346
	S-FSDT-Cubic	0.4062	0		S-FSDT-Cubic	0.4062	0
	Exact [30]	0.4062			Exact [30]	0.4062	
10^5	FSDT-Quadratic	0.3551	12.58	10^6	FSDT-Quadratic	0.3551	12.58
	S-FSDT-Quadratic	0.4056	0.1477		S-FSDT-Quadratic	0.4056	0.1477
	FSDT-Cubic	0.3556	12.4569		FSDT-Cubic	0.3551	12.58
	S-FSDT-Cubic	0.4062	0		S-FSDT-Cubic	0.4062	0
	Exact [30]	0.4062			Exact [30]	0.4062	

(b) Fully clamped

a/h	Method	$\bar{w}$	Error (%)	a/h	Method	$\bar{w}$	Error (%)
100	FSDT-Quadratic	**0.1213**	4.1107	10^3	FSDT-Quadratic	0.0252	80.0791
	S-FSDT-Quadratic	0.1244	1.6601		S-FSDT-Quadratic	0.1242	1.8182
	FSDT-Cubic	0.1268	0.2372		FSDT-Cubic	**0.1268**	0.2372
	S-FSDT-Cubic	0.1267	0.1581		S-FSDT-Cubic	0.1265	0

	Exact [30]	0.1265			Exact [30]	0.1265	
10^4	FSDT-Quadratic	3.1×10^{-4}	99.75	10^5	FSDT-Quadratic	3.2×10^{-6}	100
	S-FSDT-Quadratic	0.1242	1.8182		S-FSDT-Quadratic	0.1242	1.8182
	FSDT-Cubic	0.0674	46.7194		FSDT-Cubic	0.0014	98.8933
	S-FSDT-Cubic	0.1265	0		S-FSDT-Cubic	0.1265	0
	Exact [30]	0.1265			Exact [30]	0.1265	
10^6	FSDT -Quadratic	3.2×10^{-8}	100				
	S-FSDT-Quadratic	0.1242	1.8182				
	FSDT-Cubic	1.4×10^{-5}	99.99				
	S-FSDT-Cubic	0.1265	0				
	Exact [30]	0.1265					

Table 2. Comparisons of the normalized central deflection, bending deflections, and shear deflections obtained by the IGA based on the S-FSDT for a fully simply supported square plate.

a/h	$\bar{w}$	$\bar{w}_b$	$\bar{w}_s$
5	0.490431	0.406235	0.084196
10	0.427284	0.406235	0.021049
20	0.411497	0.406235	0.005262
50	0.407077	0.406235	8.42×10^{-4}
100	0.406446	0.406235	2.10×10^{-4}
10^3	0.406237	0.406235	2.10×10^{-6}
10^4	0.406235	0.406235	2.10×10^{-8}
10^5	0.406235	0.406235	2.10×10^{-10}

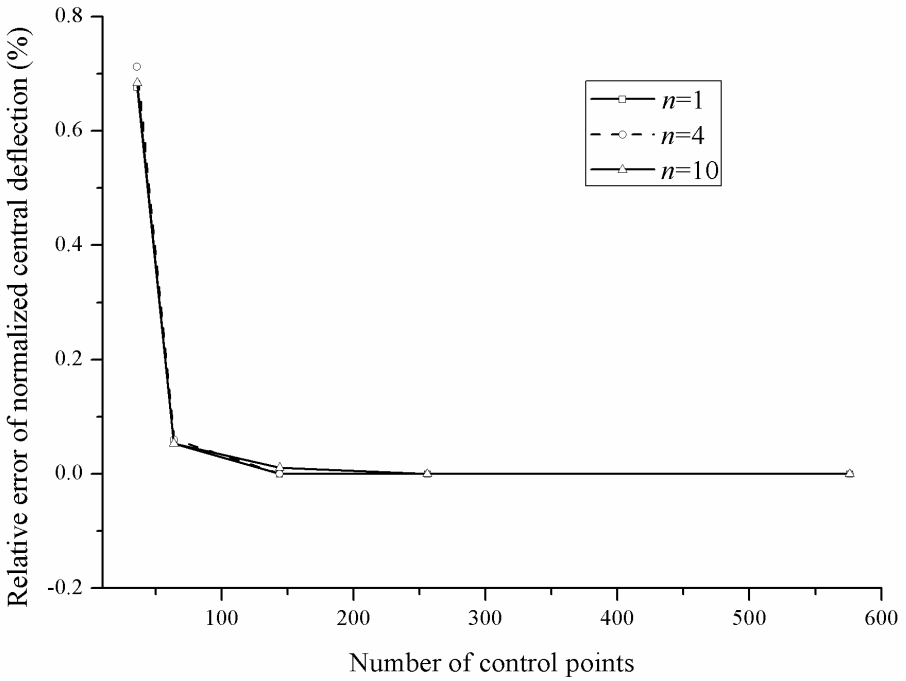

Fig. 2. Convergence results in the relative error of normalized central deflection.

Table 3. Normalized central deflections of Al/ Al_2O_3 square plate under sinusoidal loads.

Method		Number of control points	*n*=1	*n*=4	*n*=10
S-FSDT based IGA		6 × 6	0.5587	0.8227	0.9297
		8 × 8	0.5622	0.8281	0.9356
		12 × 12	0.5625	0.8286	0.9360
		16 × 16	0.5625	0.8286	0.9361
		24 × 24	0.5625	0.8286	0.9361
FSDT based IGA		16 × 16	0.5625	0.8286	0.9361
Exact	quasi-3D hyperbolic [31]	-	0.5648	0.8241	0.9228
	Higher-order theory [32]	-	0.5625	0.8286	0.9361
	S-FSDT [8]	-	0.5625	0.8286	0.9361

Table 4. Normalized central deflections of Al/Al_2O_3 square plates under sinusoidal loads.

Method		*a*/*h* =100			*a*/*h* =10			*a*/*h* =4		
		n=1	*n*=4	*n*=10	*n*=1	*n*=4	*n*=10	*n*=1	*n*=4	*n*=10
S-FSDT based IGA		0.5625	0.8286	0.9361	0.5890	0.8736	0.9966	0.7291	1.1125	1.3178
FSDT based IGA		0.5625	0.8286	0.9361	0.5890	0.8736	0.9966	0.7291	1.1125	1.3178
Exact	quasi-3D hyperbolic [31]	0.5648	0.8241	0.9228	0.5868	0.8698	0.9886	0.702	1.1095	1.3327
	Higher-order theory [32]	0.5625	0.8286	0.9361	0.5875	0.8821	1.0072	0.7171	1.1585	1.3745
	S-FSDT [8]	0.5625	0.8286	0.9361	0.5890	0.8736	0.9966	0.7291	1.1125	1.3178

Table 5. Normalized deflection of Al/ZrO_2-1 plate with different length–thickness ratios *a*/*h* and gradient indexes *n*.

Type	*a*/*h*	Method	*n*=0	*n*=0.5	*n*=1	*n*=2
SSSS	5	S-FSDT based IGA	0.1717	0.2324	0.2719	0.3115
		FSDT based IGA	0.1717	0.2324	0.2719	0.3115
		FSDT based kp-Ritz [33]	0.1722	0.2403	0.2811	0.3221
		FSDT based ES-DSG3 [34]	0.1703	0.2232	0.2522	0.2827
	20	S-FSDT based IGA	0.1440	0.1972	0.2310	0.2628
		FSDT based IGA	0.1440	0.1972	0.2310	0.2628
	100	S-FSDT based IGA	0.1423	0.1949	0.2284	0.2597
		FSDT based IGA	0.1423	0.1949	0.2284	0.2597
SFSS	5	S-FSDT based IGA	0.3164	0.4299	0.5032	0.5752
		FSDT based IGA	0.3175	0.4314	0.5049	0.5772
	20	S-FSDT based IGA	0.2800	0.3835	0.4493	0.5109
		FSDT based IGA	0.2803	0.3838	0.4497	0.5114
	100	S-FSDT based IGA	0.2777	0.3805	0.4458	0.5068
		FSDT based IGA	0.2777	0.3805	0.4458	0.5069
SFSF	5	S-FSDT based IGA	0.5083	0.6918	0.8099	0.9247
		FSDT based IGA	0.5089	0.6926	0.8108	0.9258
	20	S-FSDT based IGA	0.4614	0.6319	0.7404	0.8420
		FSDT based IGA	0.4615	0.6321	0.7406	0.8422
	100	S-FSDT based IGA	0.4584	0.6281	0.7360	0.8367
		FSDT based IGA	0.4584	0.6281	0.7360	0.8367

Table 6. Normalized deflection of Al/Al_2O_3 thin plate under different gradient indexes and boundary conditions

Type	Method	n=0	n=0.5	n=1	n=2	n=5	n=10
SSSS	S-FSDT	0.4438	0.6846	0.8904	1.1411	1.3494	1.4816
	FSDT	0.4438	0.6847	0.8904	1.1411	1.3494	1.4816
SFSF	S-FSDT	1.4302	2.2062	2.8692	3.6770	4.3483	4.7740
	FSDT	1.4302	2.2062	2.8693	3.6770	4.3483	4.7740
SCSC	S-FSDT	0.2096	0.3232	0.4204	0.5387	0.6372	0.6996
	FSDT	0.2097	0.3234	0.4205	0.5389	0.6375	0.7000
CCCC	S-FSDT	0.1384	0.2135	0.2776	0.3557	0.4208	0.4621
	FSDT	0.1384	0.2135	0.2776	0.3558	0.4209	0.4622

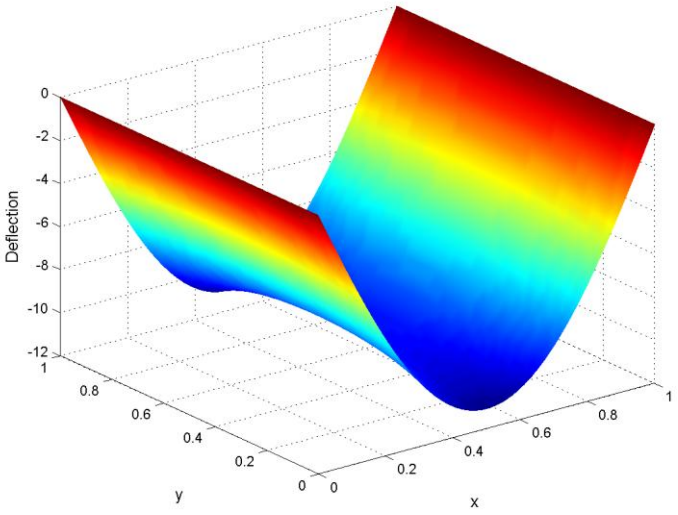
Deflection
0
-2
-4
-6
-8
-10
-12
1
0.8
0.6
0.4
0.2
0
y
0
0.2
0.4
0.6
0.8
1
x

(a)

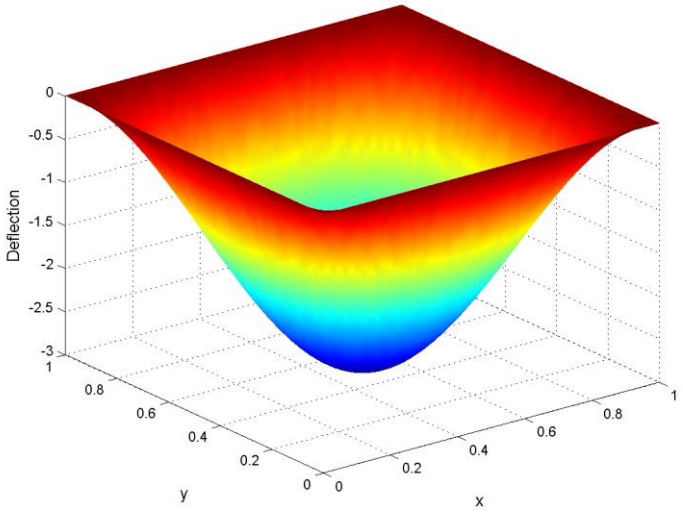
Deflection
0
-0.5
-1
-1.5
-2
-2.5
-3
1
0.8
0.6
0.4
0.2
0
y
0
0.2
0.4
0.6
0.8
1
x

(b)

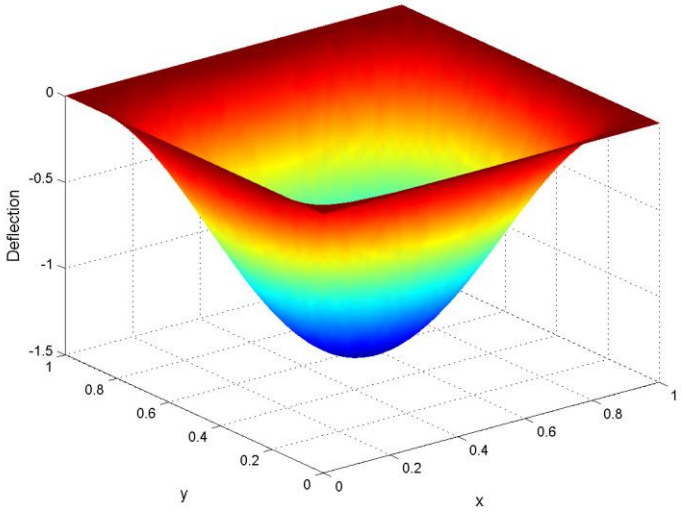

(c)

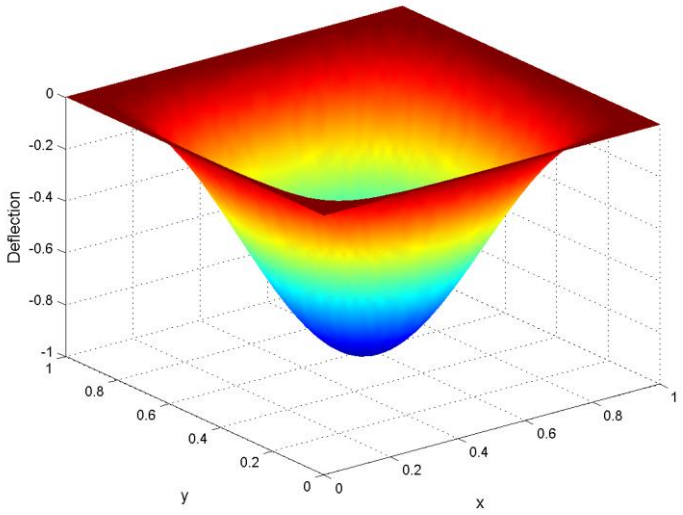

(d)

Fig. 3. Deflection of Al/Al_2O_3 thin plate with different boundary conditions (n = 2): (a) SFSF, (b) SSSS, (c) SCSC, and (d) CCCC.

Table 7. Normalized deflection for a circular plate subjected to a uniformly distributed pressure.

Boundary condition	Exact [35]	FSDT based IGA	S-FSDT based IGA	Kirchhoff theory based MLPG [35]	Error (%)		
					FSDT based IGA	S-FSDT based IGA	Kirchhoff theory based MLPG [35]
Simply supported	0.0637	0.0637	0.0634	0.0639	0.0738	0.5196	0.3265
Clamped	0.0156	0.0156	0.0156	0.0156	0.2430	0.0832	0.4160

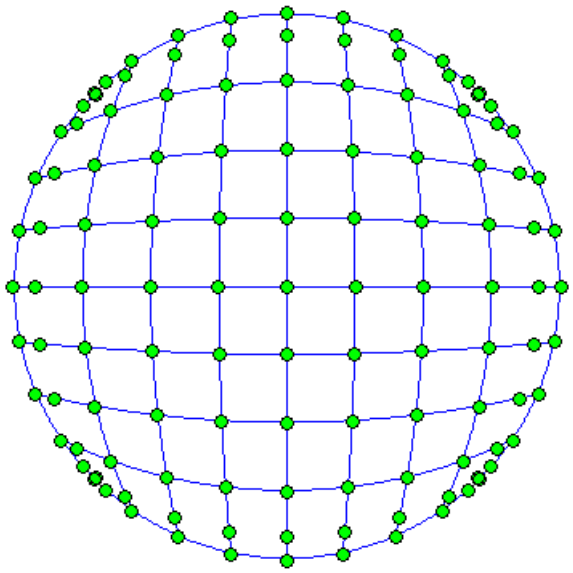

Fig. 4. Control points and physical mesh of a circular plate with cubic NURBS basis function.

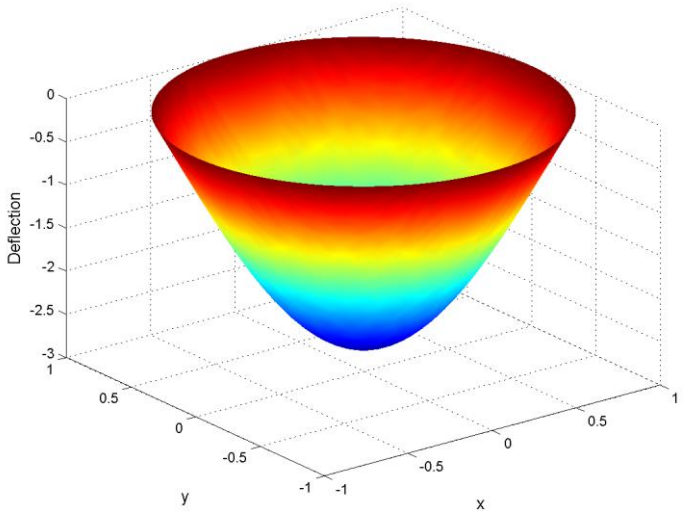

(a)

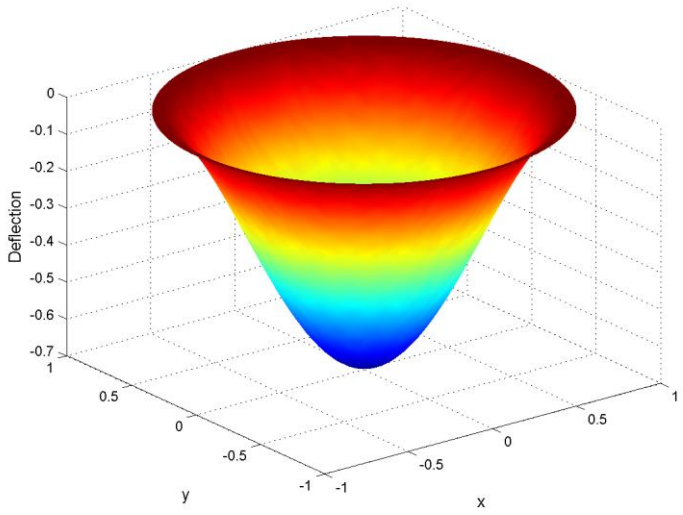

(b)

Fig. 5. Deflection of titanium/zirconium circular plate with h/R = 0.05 and n = 2: (a) roller supported; (b) clamped.

Table 8. Normalized center deflection of circular titanium/zirconium plate subjected to a uniform load.

(a) Roller supported boundary condition

h/R	Method	*n*=0	*n*=2	*n*=4	*n*=8	*n*=10	*n*=50	*n*=100	$n=10^5$
0.05	Elasticity solutions [36]	10.3910	5.7090	5.2190	4.8090	4.7000	4.2560	4.1870	4.1180
	Reddy [37]	10.3960	5.7140	5.2230	4.8120	4.7040	4.2580	4.1890	4.1180
	HSDT based IGA [15]	10.2203	5.6100	5.1299	4.7299	4.6239	4.1881	4.1198	4.0495
	FSDT based IGA	10.3963	5.7137	5.2227	4.8124	4.7036	4.2584	4.1895	4.1170
	S-FSDT based IGA	10.3411	5.4851	5.0966	4.7513	4.6542	4.2347	4.1670	4.0951
0.1	Elasticity solutions [36]	10.4600	5.7380	5.2450	4.8350	4.7270	4.2830	4.2150	4.1460
	Reddy [37]	10.4810	5.7560	5.2610	4.8480	4.7390	4.2930	4.2230	4.1510
	HSDT based IGA [15]	10.3440	5.6742	5.1879	4.7838	4.6769	4.2377	4.1690	4.0970
	FSDT based IGA	10.4817	5.7561	5.2612	4.8487	4.7394	4.2927	4.2235	4.1508
	S-FSDT based IGA	10.4262	5.5273	5.1349	4.7874	4.6899	4.2688	4.2009	4.1288
0.2	Elasticity solutions [36]	10.7360	5.8530	5.3510	4.9410	4.8330	4.3920	4.3240	4.2550
	Reddy [37]	10.8220	5.9250	5.4140	4.9930	4.8820	4.4290	4.3590	4.2860
	HSDT based IGA [15]	10.6973	5.8475	5.3439	4.9315	4.8230	4.3793	4.3098	4.2369
	FSDT based IGA	10.8223	5.9250	5.4147	4.9932	4.8821	4.4291	4.3592	4.2857
	S-FSDT based IGA	10.7667	5.6961	5.2883	4.9319	4.8326	4.4052	4.3365	4.2637

(b) Clamped boundary condition

h/R	Method	*n*=0	*n*=2	*n*=4	*n*=8	*n*=10	*n*=50	*n*=100	$n=10^5$
0.05	Elasticity solutions [36]	2.561	1.4050	1.2840	1.1840	1.1570	1.0490	1.0320	1.0150
	Reddy [37]	2.554	1.4020	1.2820	1.1810	1.1550	1.0460	1.0290	1.0110
	HSDT based IGA [15]	2.548	1.3990	1.2786	1.1785	1.1520	1.0435	1.0267	1.0092
	FSDT based IGA	2.5539	1.4024	1.2819	1.1814	1.1547	1.0459	1.0291	1.0114
	S-FSDT based IGA	2.5535	1.4023	1.2817	1.1812	1.1546	1.0458	1.0289	1.0112

0.1	Elasticity solutions [36]	2.667	1.4560	1.3290	1.2270	1.2010	1.0910	1.0740	1.0570
	Reddy [37]	2.639	1.4440	1.3200	1.2170	1.1900	1.0800	1.0630	1.0450
	HSDT based IGA [15]	2.6297	1.4386	1.3143	1.2123	1.1855	1.0762	1.0592	1.0415
	FSDT based IGA	2.6393	1.4448	1.3203	1.2176	1.1905	1.0801	1.0631	1.0452
	S-FSDT based IGA	2.6353	1.4428	1.3186	1.2159	1.1889	1.0785	1.0615	1.0436
0.2	Elasticity solutions [36]	3.093	1.6580	1.5110	1.4020	1.3750	1.2620	1.2440	1.2260
	Reddy [37]	2.979	1.6130	1.4730	1.3620	1.3330	1.2160	1.1990	1.1800
	HSDT based IGA [15]	2.9541	1.5958	1.4557	1.3467	1.3187	1.2060	1.1884	1.1700
	FSDT based IGA	2.9799	1.6137	1.4738	1.3622	1.3332	1.2166	1.1988	1.1800
	S-FSDT based IGA	2.9625	1.6051	1.4659	1.3548	1.3260	1.2097	1.1918	1.1732

Table 9. First normalized natural frequency of Al/Al_2O_3 square plate for $a/h = 5$.

Method		Number of control points	n=1	n=4	n=10
S-FSDT based IGA		6 × 6	0.1625	0.1391	0.1321
		8 × 8	0.1625	0.1389	0.1320
		12 × 12	0.1624	0.1390	0.1320
		16 × 16	0.1624	0.1390	0.1320
		24 × 24	0.1624	0.1390	0.1320
FSDT based IGA		16 × 16	0.1630	0.1398	0.1323
Exact	2D-HOT [38]	-	0.1640	0.1383	0.1306
	S-HSDT [39]	-	0.1631	0.1378	0.1301
	S-FSDT based FEM [40]	-	0.1629	0.1396	0.1322

Table 10. First normalized natural frequency of Al/Al_2O_3 square plate for a/h = 2, 10, 20.

a/h	Method		n=0	n=0.5	n=1	n=4	n=10
2	Analytical solutions	2D-HOT [38]	0.9400	0.8232	0.7476	0.5997	0.5460
		S-HSDT [39]	0.9297	0.8110	0.7356	0.5924	0.5412
	S-FSDT based FEM [40]		0.9255	0.8052	0.7330	0.6115	0.5642
	FSDT based IGA		0.9265	0.8060	0.7330	0.6111	0.5640
	S-FSDT based IGA		0.9265	0.8027	0.7267	0.6055	0.5620
10	Analytical solutions	2D-HOT [38]	0.0578	0.0492	0.0443	0.0381	0.0364
		S-HSDT [39]	0.0577	0.0490	0.0442	0.0381	0.0364
	S-FSDT based FEM [40]		0.0576	0.0489	0.0441	0.0382	0.0365
	FSDT based IGA		0.0577	0.0490	0.0442	0.0382	0.0366
	S-FSDT based IGA		0.0577	0.0490	0.0441	0.0382	0.0365
20	2D-HOT based analytical solutions [38]		0.0148	0.0125	0.0113	0.0098	0.0094
	FSDT based element-free kp-Ritz method [41]		0.0146	0.0124	0.0112	0.0097	0.0093
	S-FSDT based FEM [40]		0.0148	0.0125	0.0113	0.0098	0.0094
	FSDT based IGA		0.0148	0.0125	0.0113	0.00981	0.0094
	S-FSDT based IGA		0.0148	0.0125	0.0113	0.00981	0.0094

Table 11. First five mode normalized natural frequencies of Al/Al_2O_3 thin plate with various boundary conditions and gradient indexes.

(a) SFSF

n	Method	Mode 1	Mode 2	Mode 3	Mode 4	Mode 5
0	CPT-neu based IGA [42]	56.5660	94.7565	215.6539	228.7079	274.4598
	FSDT based IGA	56.5526	94.6609	215.3651	228.5948	274.1872
	S-FSDT based IGA	56.5584	94.7388	215.5711	228.5829	274.2876
	Exact [43]	56.4791	94.7141	215.6299	-	-
0.5	CPT-neu based IGA [42]	47.8972	80.2349	182.6041	193.6578	232.3979
	FSDT based IGA	47.8872	80.1627	182.3880	193.5819	232.2005
	S-FSDT based IGA	47.8913	80.2210	182.5386	193.5617	232.2649
	Exact [43]	47.7452	80.1576	182.4411	-	-
1	CPT-neu based IGA [42]	43.1596	72.2984	164.5401	174.5012	209.4085
	FSDT based IGA	43.1511	72.2369	164.3570	174.4412	209.2445
	S-FSDT based IGA	43.1544	72.2861	164.4815	174.4179	209.2924
	Exact [43]	43.0872	72.2001	164.3911	-	-
2	CPT-neu based IGA [42]	39.2395	65.7314	149.5922	158.6496	190.3849
	FSDT based IGA	39.2316	65.6747	149.4233	158.5933	190.2330
	S-FSDT based IGA	39.2347	65.7197	149.5365	158.5722	190.2767
	Exact [43]	39.1666	65.6400	149.0583	-	-

(b) SSSS

n	Method	Mode 1	Mode 2	Mode 3	Mode 4	Mode 5
0	CPT-neu based IGA [42]	115.9253	289.7845	289.7845	463.5955	579.5359
	FSDT based IGA	115.8932	289.6145	289.6145	463.1163	579.2636
	S-FSDT based IGA	115.8926	289.5806	289.5806	463.0741	578.7215

	Exact [43]	115.8695	289.7708	-	463.4781	-
0.5	CPT-neu based IGA [42]	98.1595	245.3740	245.3740	392.5471	490.7185
	FSDT based IGA	98.1354	245.2532	245.2532	392.195	490.6291
	S-FSDT based IGA	98.1343	245.2169	245.2169	392.1448	490.0963
	Exact [43]	98.0136	245.3251	-	392.4425	-
1	CPT-neu based IGA [42]	88.4501	221.1011	221.1011	353.7127	442.1697
	FSDT based IGA	88.4296	221.0019	221.0019	353.4173	442.1505
	S-FSDT based IGA	88.428	220.9643	220.9643	353.3613	441.6348
	Exact [43]	88.3093	221.0643	-	353.6252	-
2	CPT-neu based IGA [42]	80.4160	201.0155	201.0155	321.5761	401.9929
	FSDT based IGA	80.3972	200.9234	200.9234	321.3032	401.9628
	S-FSDT based IGA	80.3953	200.8879	200.8879	321.2475	401.5008
	Exact [43]	80.3517	200.8793	-	321.4069	-

(c) SCSC

n	Method	Mode 1	Mode 2	Mode 3	Mode 4	Mode 5
0	CPT-neu based IGA [42]	170.0240	321.4690	407.1180	555.3781	600.2165
	FSDT based IGA	169.8890	321.1655	406.5798	554.3949	599.7747
	S-FSDT based IGA	169.9230	321.1937	406.5707	554.5021	599.3170
	Exact [43]	170.0196	321.4069	-	555.2809	-
0.5	CPT-neu based IGA [42]	143.9675	272.2028	344.7257	470.2635	508.2296
	FSDT based IGA	143.8672	271.9835	344.3519	469.5518	508.0145
	S-FSDT based IGA	143.8904	271.9916	344.3090	469.5928	507.5430
	Exact [43]	143.8179	272.1090	-	470.0770	-
1	CPT-neu based IGA [42]	129.7269	245.2758	310.6242	423.7400	457.9482
	FSDT based IGA	129.6422	245.0938	310.3216	423.1484	457.8229
	S-FSDT based IGA	129.6605	245.0927	310.2664	423.1599	457.3585

	Exact [43]	129.6496	245.1310	-	423.6904	-
2	CPT-neu based IGA [42]	117.9435	222.9939	282.4052	385.2402	416.3375
	FSDT based IGA	117.8652	222.8253	282.1232	384.6922	416.2095
	S-FSDT based IGA	117.8818	222.8238	282.0750	384.7018	415.7952
	Exact [43]	117.8104	222.8111	-	385.0672	-

(d) CCCC

n	Method	Mode 1	Mode 2	Mode 3	Mode 4	Mode 5
0	CPT-neu based IGA [42]	211.3372	431.0061	431.0061	635.4464	772.7523
	FSDT based IGA	211.1203	430.3532	430.3532	633.9937	771.9821
	S-FSDT based IGA	211.1468	430.3633	430.3633	634.1625	770.8950
0.5	CPT-neu based IGA [42]	178.9493	364.9528	364.9528	538.0607	654.3228
	FSDT based IGA	178.7886	364.4940	364.4940	537.0131	654.0679
	S-FSDT based IGA	178.8047	364.4639	364.4639	537.0816	652.9193
1	CPT-neu based IGA [42]	161.2484	328.8502	328.8502	484.8293	589.5860
	FSDT based IGA	161.1129	328.4760	328.4760	483.9606	589.5289
	S-FSDT based IGA	161.1242	328.4308	328.4308	483.9866	588.3962
2	CPT-neu based IGA [42]	146.6016	298.9753	298.9753	440.7781	536.0119
	FSDT based IGA	146.4765	298.6270	298.6270	439.9730	535.9244
	S-FSDT based IGA	146.4868	298.5884	298.5884	439.9988	534.9293

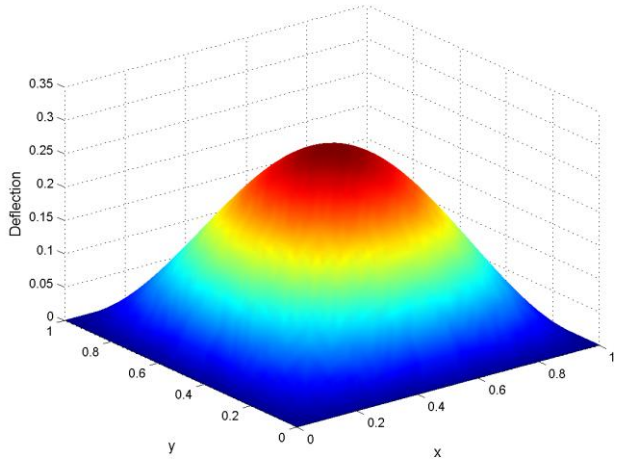
Deflection
0.35
0.3
0.25
0.2
0.15
0.1
0.05
0
y
x

(a)

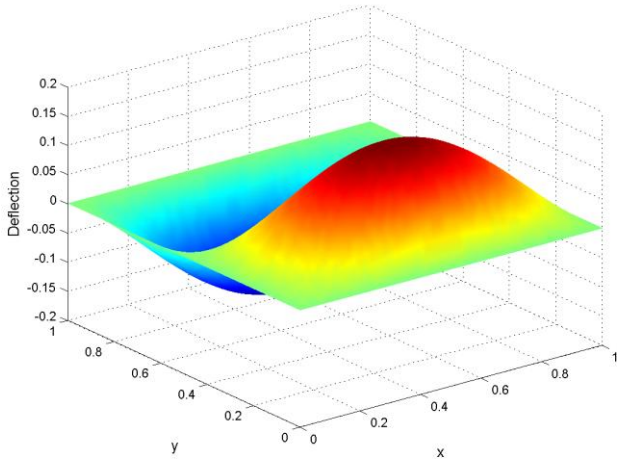
Deflection
0.2
0.15
0.1
0.05
0
-0.05
-0.1
-0.15
-0.2
y
x

(b)

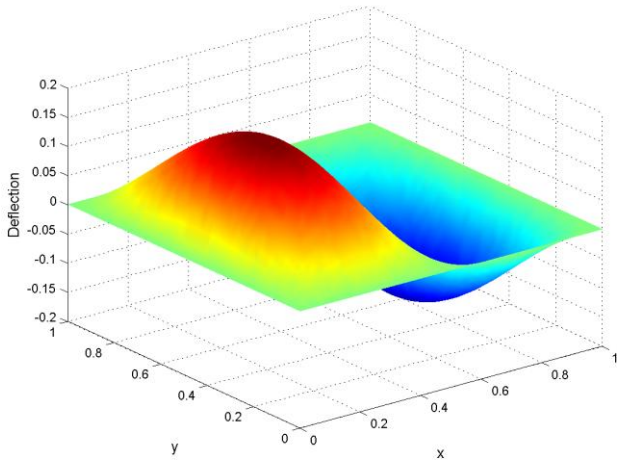
Deflection
0.2
0.15
0.1
0.05
0
-0.05
-0.1
-0.15
-0.2
y
x

(c)

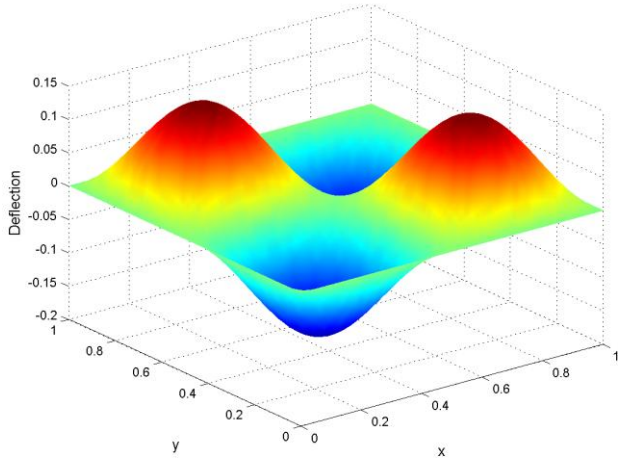

(d)

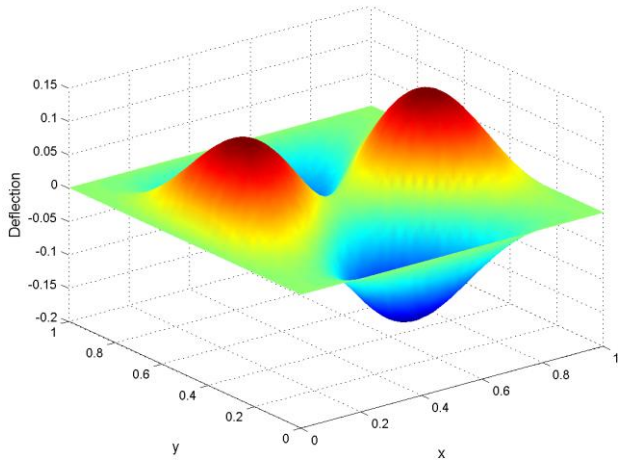

(e)

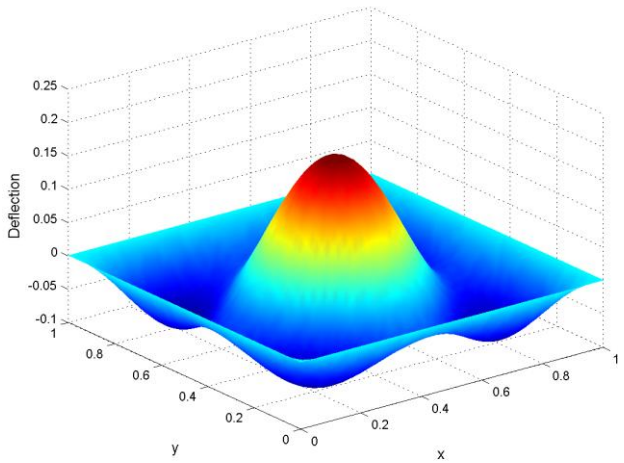

(f)

Fig. 6. First six mode shapes of simply supported Al/Al_2O_3 thin plate: (a) mode 1, (b) mode 2, (c) mode 3, (d) mode 4, (e) mode 5, and (f) mode 6.

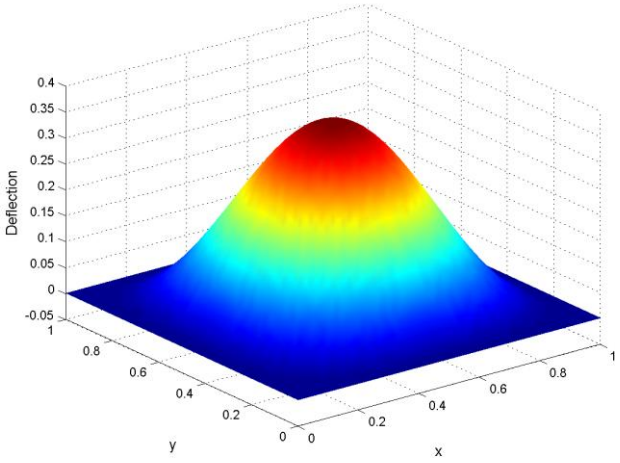
Deflection
0.4
0.35
0.3
0.25
0.2
0.15
0.1
0.05
0
-0.05
1
0.8
0.6
0.4
0.2
0
y
0
0.2
0.4
0.6
0.8
1
x

(a)

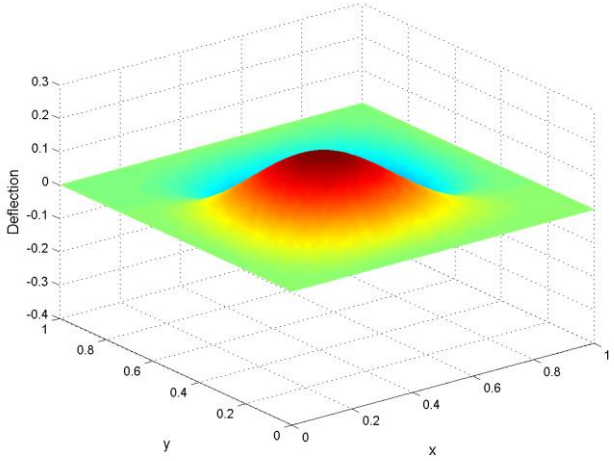
Deflection
0.3
0.2
0.1
0
-0.1
-0.2
-0.3
-0.4
1
0.8
0.6
0.4
0.2
0
y
0
0.2
0.4
0.6
0.8
1
x

(b)

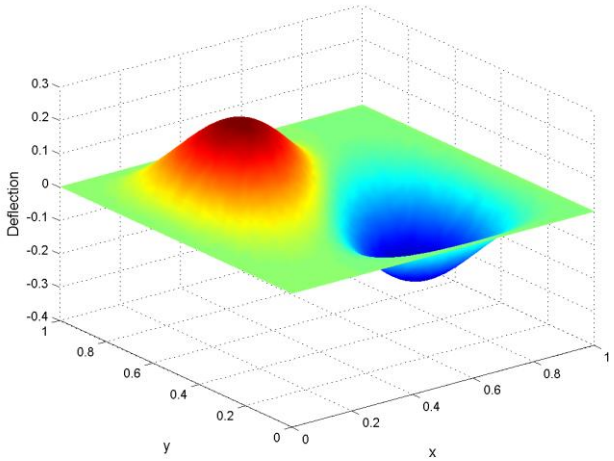
Deflection
0.3
0.2
0.1
0
-0.1
-0.2
-0.3
-0.4
1
0.8
0.6
0.4
0.2
0
y
0
0.2
0.4
0.6
0.8
1
x

(c)

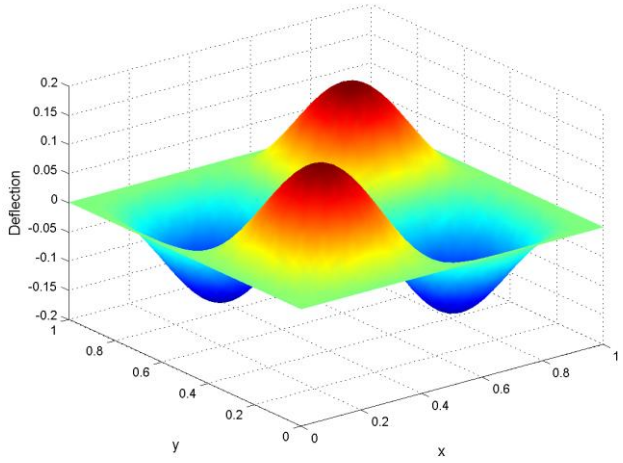

(d)

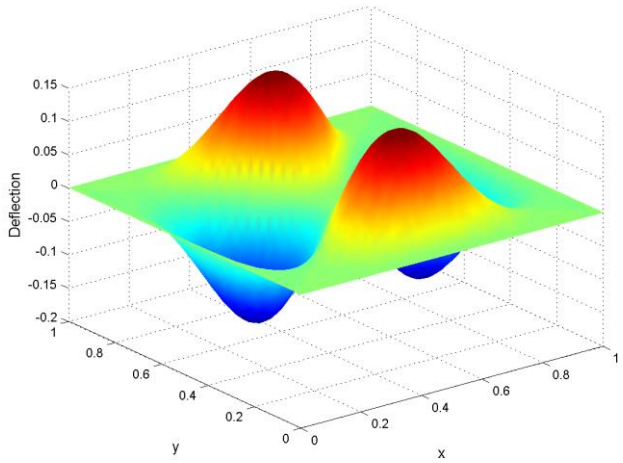

(e)

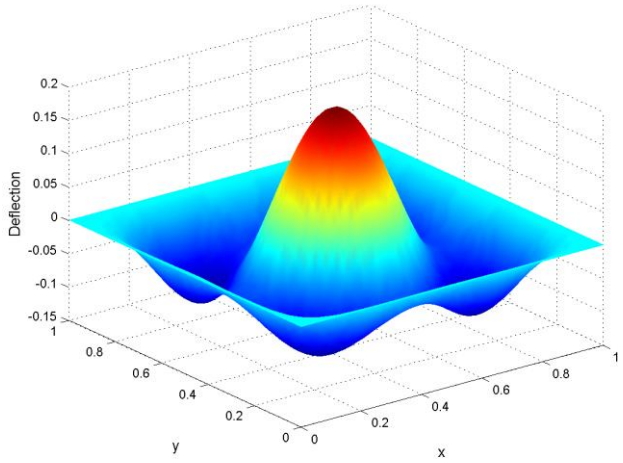

(f)

Fig. 7. First six mode shapes of clamped Al/Al_2O_3 thin plate: (a) mode 1, (b) mode 2, (c) mode 3, (d) mode 4, (e) mode 5, and (f) mode 6.

Table 12. First six frequencies of circular Al/Al_2O_3 plate with clamped edge (n = 1).

h/R	Method	Mode 1	Mode 2	Mode 3	Mode 4	Mode 5	Mode 6
0.01	semi-analytical [44]	0.0236	0.0491	0.0805	0.0918	0.1178	0.1404
	FEM [45]	0.0234	0.0486	0.0798	0.0909	0.1167	0.1391
	UM [45]	0.0257	0.0535	0.0877	0.1000	0.1283	0.1529
	HSDT based IGA [15]	0.0236	0.0492	0.0807	0.0924	0.1191	0.1431
	FSDT based IGA	0.0237	0.0511	0.0855	0.0997	0.1101	0.1451
	S-FSDT based IGA	0.0236	0.0491	0.0805	0.0919	0.1180	0.1408
0.1	semi-analytical [44]	2.3053	4.6934	7.5146	8.5181	10.7128	12.6197
	FEM [45]	2.2888	4.6661	7.4808	8.4829	10.6776	12.5877
	UM [45]	2.5038	5.0831	8.1156	9.1931	11.5376	13.5743
	IGA with HSDT [15]	2.3076	4.7005	7.5318	8.5380	10.7483	12.6636
	IGA with FSDT	2.3042	4.6936	7.5190	8.5472	10.7923	12.8097
	IGA with S-FSDT	2.3040	4.7137	7.5773	8.5244	10.8524	12.7017
0.2	semi-analytical [44]	8.6535	16.7666	25.6486	28.7574	34.0756	35.0981
	FEM [45]	8.6403	16.7890	25.7661	28.9152	34.1893	35.3618
	UM [45]	9.3162	17.9164	27.2480	30.4998	–	37.1197
	IGA with HSDT [15]	8.6787	16.8595	25.8479	29.0092	34.0581	35.4875
	IGA with FSDT	8.6490	16.7604	25.6426	28.7732	34.0571	35.1592
	IGA with S-FSDT	8.6486	17.0016	26.2512	28.7691	34.1216	36.1557

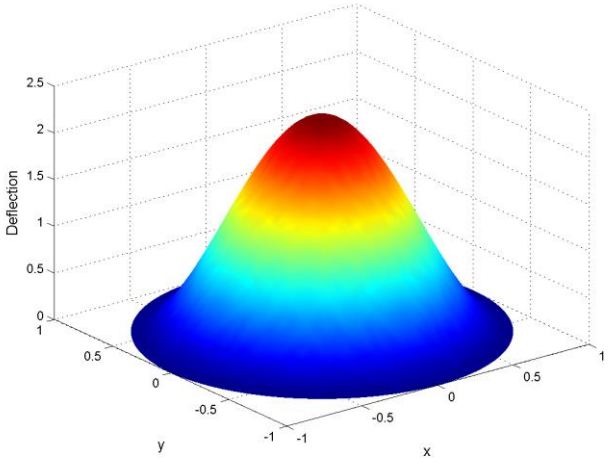
Deflection
2.5
2
1.5
1
0.5
0
1
0.5
0
-0.5
-1
y
-1
-0.5
0
0.5
1
x

(a)

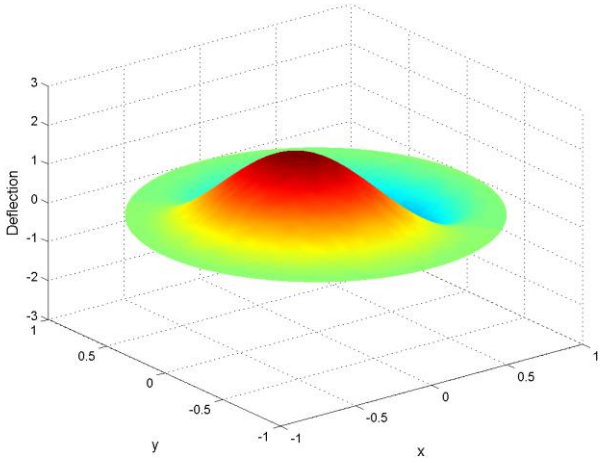
Deflection
3
2
1
0
-1
-2
-3
1
0.5
0
-0.5
-1
y
-1
-0.5
0
0.5
1
x

(b)

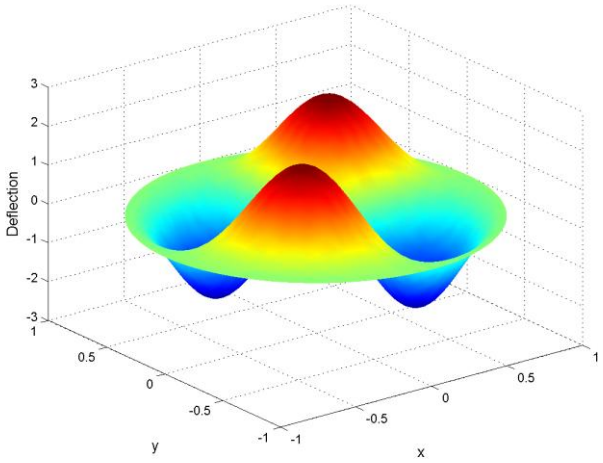
Deflection
3
2
1
0
-1
-2
-3
1
0.5
0
-0.5
-1
y
-1
-0.5
0
0.5
1
x

(c)

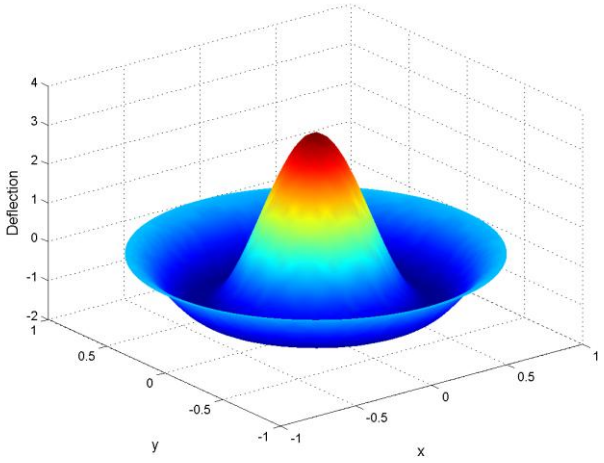

(d)

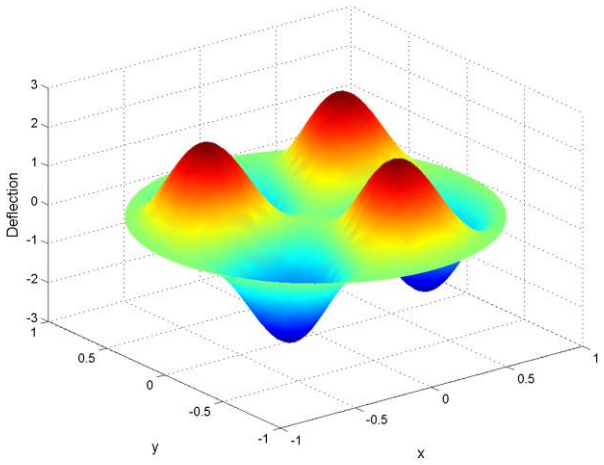

(e)

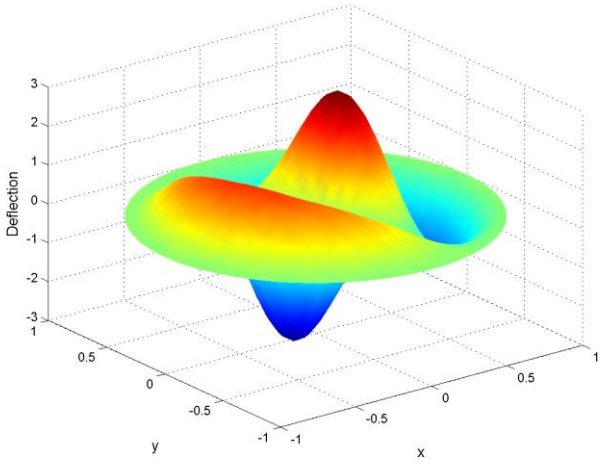

(f)

Fig. 8. First six mode shapes of clamped Al/Al_2O_3 circular plate with R/h = 0.01 and n = 1: (a) mode 1, (b) mode 2, (c) mode 3, (d) mode 4, (e) mode 5, and (f) mode 6.

Table 13. First normalized frequency of Al/Al_2O_3 circular plate with R/h =0.01

Boundary condition	Method	n=0	n=1	n=2	n=5	n=10
Free	FSDT based IGA	0.01623	0.01239	0.01126	0.01067	0.01034
	S-FSDT based IGA	0.01618	0.01234	0.01122	0.01064	0.01030
Simply supported	FSDT based IGA	0.01495	0.01141	0.01037	0.00983	0.00952
	S-FSDT based IGA	0.01498	0.01214	0.01142	0.01071	0.01002
Clamped	FSDT based IGA	0.03106	0.02372	0.02156	0.02043	0.01977
	S-FSDT based IGA	0.03090	0.02358	0.02144	0.02033	0.01968

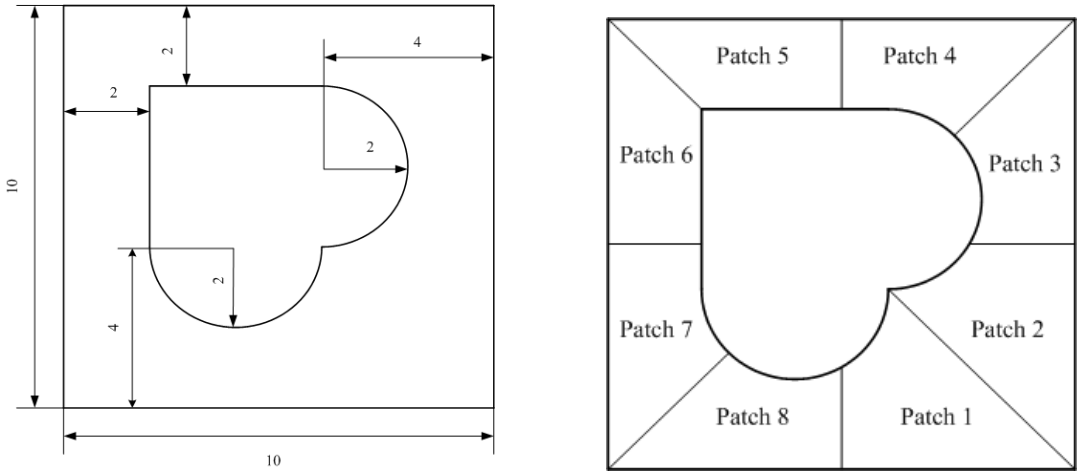

Fig. 9. A thin square plate with a complicated cutout: geometric parameters (left) and discretization of the patches (right).

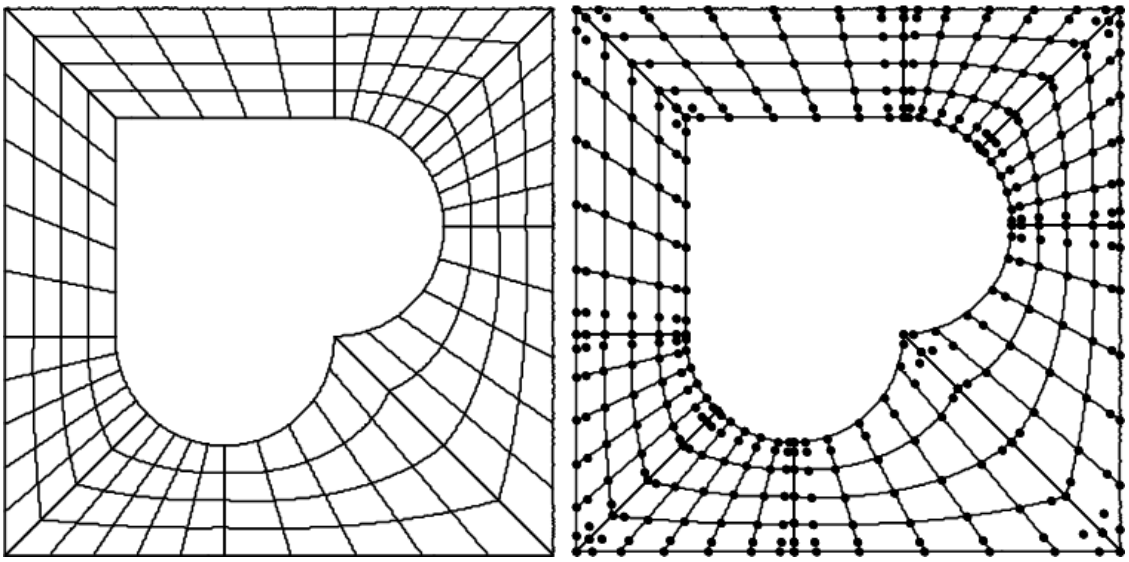

Fig. 10. Physical meshes (left) and control points (right).

Table 14. Normalized natural frequencies of thin square plate with a complicated cutout.

(a) SSSS

Mode	Kirchhoff based IGA [47]	MKI [48]	EFG [49]	NS-RPIM [50]	FSDT based IGA	S-FSDT based IGA
1	5.193	5.390	5.453	4.919	4.914	5.098
2	6.579	7.502	8.069	6.398	6.390	6.608
3	6.597	8.347	9.554	6.775	6.762	6.929
4	7.819	10.636	10.099	8.613	8.568	8.644
5	8.812	11.048	11.328	9.016	8.982	9.031
6	9.420	12.894	12.765	10.738	10.683	10.591
7	10.742	13.710	13.685	10.93	10.934	10.946
8	10.776	14.062	14.305	11.601	11.694	11.800
9	11.919	16.649	15.721	12.903	12.852	12.517
10	13.200	17.364	17.079	13.283	13.229	13.001

(b) CCCC

Mode	Kirchhoff based IGA [47]	EFG [49]	NS-RPIM [50]	FSDT based IGA	S-FSDT based IGA
1	7.621	7.548	7.410	7.453	7.431
2	9.810	10.764	9.726	9.825	9.880
3	9.948	11.113	9.764	9.845	9.992
4	11.135	11.328	10.896	10.964	11.077
5	11.216	12.862	11.114	11.165	11.254
6	12.482	13.300	12.353	12.381	12.424
7	12.872	14.168	12.781	12.953	12.862
8	13.650	15.369	13.368	13.721	13.678
9	14.676	16.205	14.485	14.511	14.227
10	14.738	17.137	14.766	14.792	14.613

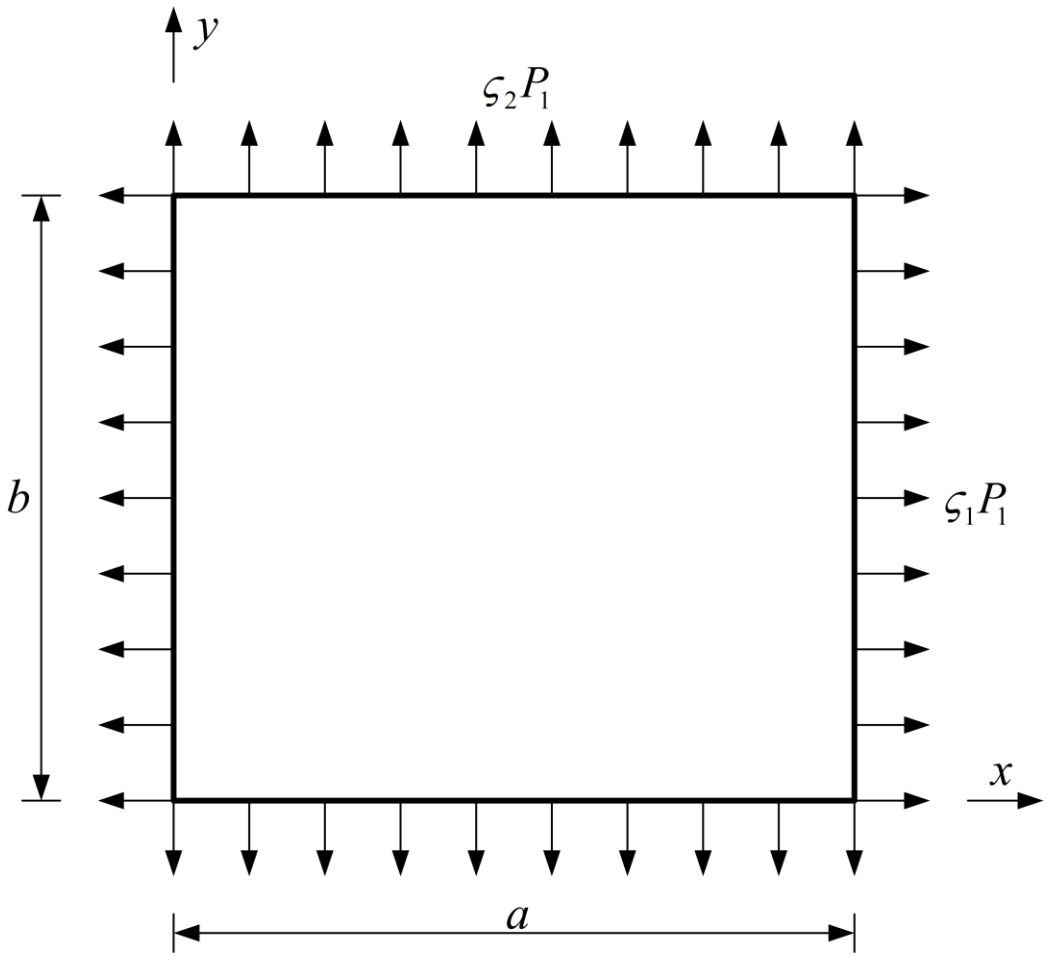

Fig. 11. A rectangular plate subjected to in-plane loads.

Table 15. Normalized buckling loads for a homogeneous rectangular plate with different boundary conditions and aspect ratios (b/h = 0.01).

Boundary condition	a/b	$(\varsigma_1, \varsigma_2)$	S-FSDT based IGA	Levy [51]	Levy [52]
SSSS	0.5	-1,0	15.4200	15.42	15.4212
		-1,-1	12.3358	12.33	12.337
	1	-1,0	39.4720	39.23	39.4784
		-1,-1	19.7360	19.74	19.7392
SCSC	0.5	-1,0	18.9763	18.97	18.9775
		-1,-1	14.6158	14.62	14.6174
	1	-1,0	75.8831	75.92	75.9099
		-1,-1	37.7886	37.8	37.7996
SFSF	0.5	-1,0	9.6040	9.604	9.6047
		-1,-1	9.3999	9.4	9.4006
	1	-1,0	9.3982	9.4	9.3989
		-1,-1	9.1997	9.199	9.2005

Table 16. Buckling loads (*MN/m*) for the Al /Al_2O_3 plate with different boundary conditions and aspect ratios.

(a) SFSF

n	*a/b*	Method	$(\varsigma_1, \varsigma_2)$		
			1,0	0,1	1,1
0	0.5	S-FSDT based IGA	1.33648	3.10375	1.30806
		Levy [52]	1.33691	3.10571	1.30852
	1	S-FSDT based IGA	0.32704	0.70153	0.32014
		Levy [52]	0.32707	0.701642	0.32016
	1.5	S-FSDT based IGA	0.14316	0.26184	0.14081
		Levy [52]	0.14316	0.26185	0.15264
1	0.5	S-FSDT based IGA	0.66612	1.54693	0.72216
		Levy [52]	0.66637	1.54801	0.72251
	1	S-FSDT based IGA	0.16301	0.34967	0.15957
		Levy [52]	0.16302	0.34973	0.17119
	1.5	S-FSDT based IGA	0.07136	0.13051	0.07019
		Levy [52]	0.07136	0.13052	0.07019
2	0.5	S-FSDT based IGA	0.51977	1.20704	0.50871
		Levy [52]	0.51998	1.20794	0.50894
	1	S-FSDT based IGA	0.12720	0.27285	0.12451
		Levy [52]	0.12721	0.27290	0.12452
	1.5	S-FSDT based IGA	0.05568	0.10184	0.05477
		Levy [52]	0.05568	0.10185	0.05477

(b) SSSS

n	*a/b*	Method	$(\varsigma_1, \varsigma_2)$		
			1,0	0,1	1,1
0	0.5	S-FSDT based IGA	2.14581	8.58058	1.71654
		Levy [52]	2.14655	8.58619	1.71724
	1	S-FSDT based IGA	1.37357	1.37357	0.68678
		Levy [52]	1.37379	1.37379	0.68689
	1.5	S-FSDT based IGA	1.49042	0.71653	0.49603
		Levy [52]	1.49066	0.71658	0.49609
1	0.5	S-FSDT based IGA	1.06949	4.27663	0.85554
		Levy [52]	1.06993	4.27971	0.85594
	1	S-FSDT based IGA	0.68463	0.68463	0.34231
		Levy [52]	0.68475	0.684753	0.34238
	1.5	S-FSDT based IGA	0.74286	0.35714	0.24724
		Levy [52]	0.743	0.35717	0.24727
2	0.5	S-FSDT based IGA	0.83450	3.33699	0.66756

		Levy [52]	0.83488	3.33953	0.66791
	1	S-FSDT based IGA	0.53422	0.53422	0.26711
		Levy [52]	0.53432	0.53432	0.26716
	1.5	S-FSDT based IGA	0.57966	0.27868	0.19292
		Levy [52]	0.57978	0.27871	0.19295

(c)SCSC

n	*a/b*	Method	$(\varsigma_1, \varsigma_2)$		
			1,0	0,1	1,1
0	0.5	S-FSDT based IGA	2.64052	6.65596	2.03369
		Levy [52]	2.64155	6.65897	2.03466
	1	S-FSDT based IGA	2.64062	2.31569	1.31499
		Levy [52]	2.64155	2.31593	1.31537
	1.5	S-FSDT based IGA	2.44312	1.72986	1.29362
		Levy [52]	2.44395	1.72987	1.29397
1	0.5	S-FSDT based IGA	1.31606	3.31722	1.01360
		Levy [52]	1.31666	3.3191	1.01416
	1	S-FSDT based IGA	1.31612	1.15417	0.65541
		Levy [52]	1.31666	1.15435	0.65563
	1.5	S-FSDT based IGA	1.21771	0.86219	0.64477
		Levy [52]	1.2181	0.86224	0.64496
2	0.5	S-FSDT based IGA	1.02691	2.58828	0.79089
		Levy [52]	1.02741	2.58995	0.79136
	1	S-FSDT based IGA	1.02696	0.90059	0.51141
		Levy [52]	1.02741	0.90076	0.511603
	1.5	S-FSDT based IGA	0.95018	0.67276	0.50311
		Levy [52]	0.95056	0.67282	0.50328